Silica nanoparticles induce cardiotoxicity interfering with energetic status and Ca2+ handling in adult rat cardiomyocytes

Article *in* AJP Heart and Circulatory Physiology · January 2017

DOI: 10.1152/ajpheart.00564.2016

CITATIONS
6

READS
134

13 authors, including:

Enrique Guerrero-Beltrán
Tecnológico de Monterrey
20 PUBLICATIONS **414** CITATIONS
SEE PROFILE

Judith Bernal-Ramírez
Tecnológico de Monterrey
14 PUBLICATIONS **38** CITATIONS
SEE PROFILE

Omar Lozano
Tecnológico de Monterrey
50 PUBLICATIONS **249** CITATIONS
SEE PROFILE

Yuriana Oropeza-Almazán
Rush University Medical Center
18 PUBLICATIONS **116** CITATIONS
SEE PROFILE

Articles in PresS. Am J Physiol Heart Circ Physiol (January 27, 2017). doi:10.1152/ajpheart.00564.2016

Silica nanoparticles induce cardiotoxicity interfering with energetic status and Ca^{2+} handling in adult rat cardiomyocytes

Carlos Enrique Guerrero-Beltrán[1,2], Judith Bernal-Ramírez[1,^], Omar Lozano[1,3,^], Yuriana Oropeza-Almazán[1], Elena C. Castillo[1], Jesús Roberto Garza[1], Noemí García[1,2], Jorge Vela[1], Alejandra García-García[5], Eduardo Ortega[4], Guillermo Torre-Amione[1,2,6], Nancy Ornelas-Soto[7], Gerardo García-Rivas[1,2,*]

[1]Cátedra de Cardiología y Medicina Vascular, Escuela Nacional de Medicina, Tecnológico de Monterrey. Monterrey, México.

[2]Centro de Investigación Biomédica, Hospital Zambrano-Hellion. Tecnológico de Monterrey. San Pedro Garza-García. México.

[3]Namur Nanosafety Centre (NNC), Namur Research Institute for LIfe Sciences (NARILIS), Research Centre for the Physics of Matter and Radiation (PMR), University of Namur, Namur, Belgium.

[4]Department of Physics and Astronomy, The University of Texas at San Antonio.

[5]Centro de Investigación en Materiales Avanzados S.C. Unidad Monterrey, Apodaca Nuevo León, México.

[6]Methodist DeBakey Heart & Vascular Center, The Methodist Hospital. Houston, USA.

[7]Laboratorio de Nanotecnología Ambiental, Centro del Agua. Tecnológico de Monterrey. Monterrey, México.

^ contributed equally to this work

Running title: Cardiotoxicity of silica nanoparticles

Word count of manuscript: 11,220; **Total Figures:** 11: **Total Tables:** 1

*Corresponding author

Dr. G. García-Rivas.

Hospital Zambrano-Hellion 2do. Piso. Batallón de San Patricio 112. Valle de San Agustín, San Pedro Garza-García. CP 66278, Nuevo León. México

Email: gdejesus@itesm.mx; Phone: +52 (81) 88880472; Fax: +52 (81) 88882223

Author contributions

Conception and design of research: C.E.G.B. and G.G.R.

Performed experiments: C.E.G.B., J.B.R., O.L., Y.O.A., E.C.C., J.R.G., N.G., J.V., E.O., A.G.G., N.O.S.

Analyzed data: C.E.G.B., J.B.R., O.L., Y.O.A., E.C.C,

Drafted manuscript: C.E.G.B. and G.G.R.

Interpreted results of experiments: C.E.G.B., J.B.R., O.L., E.C.C., G.T.A., G.G.R

Prepared figures: J.B.R.

Edited and revised manuscript: C.E.G.B., O.L., G.T.A., G.G.R.

Approved final version of manuscript: C. E. G.B and G.G.R.

Abstract

Recent evidence has shown that nanoparticles that have been used to improve or create new functional properties for common products may pose potential risks to human health. Silicon dioxide (SiO_2) has emerged as a promising therapy vector for the heart. However, its potential toxicity and mechanisms of damage remain poorly understood. This study provides the first exploration of SiO_2-induced toxicity in cultured cardiomyocytes exposed to 7 nm or 670 nm SiO_2 particles. We evaluated the mechanism of cell death in isolated adult cardiomyocytes exposed to 24 h incubation. The SiO_2 cell-membrane association and internalization were analyzed. SiO_2 showed a dose-dependent cytotoxic

effect with a half-maximal inhibitory concentration for the 7 nm (99.5 ± 12.4 μg/ml) and 670 nm (>1500 μg/ml) particles, which indicates size-dependent toxicity. We evaluated cardiomyocyte shortening and intracellular Ca^{2+} handling, which showed impaired contractility and intracellular Ca^{2+} transient amplitude during β-adrenergic stimulation in SiO_2 treatment. The time to 50% Ca^{2+} decay increased 39%, and the Ca^{2+} spark frequency and amplitude decreased by 35% and 21%, respectively, which suggest a reduction in sarcoplasmic reticulum Ca^{2+}-ATPase (SERCA) activity. Moreover, SiO_2 treatment depolarized the mitochondrial membrane potential and decreased ATP production by 55%. Significant glutathione depletion and H_2O_2 generation were also observed. These data indicate that SiO_2 increases oxidative stress, which leads to mitochondrial dysfunction and low energy status; these underlie reduced SERCA activity, shortened Ca^{2+} release, and reduced cell shortening. This mechanism of SiO_2 cardiotoxicity potentially plays an important role in the pathophysiology mechanism of heart failure, arrhythmias, and sudden death.

Keywords: Cardiomyocyte; silicon dioxide; nanoparticle; toxicity; Ca^{2+}

New & Noteworthy

Silica particles are used as novel nanotechnology-based vehicles for diagnostics and therapeutics for the heart. However, their potential hazardous effects remain unknown. Here, the cardiotoxicity of silica nanoparticles in rat myocytes has been described for the first time, showing an impairment of mitochondrial function that interfered directly with Ca^{2+} handling.

Introduction

The technological advances of the 20th century have been the most powerful and fastest phenomena in human history. From the largest to the smallest artifacts, newly developed micro/nanomaterials

have provided the main base for creating better and more versatile items in almost every area of knowledge. In this regard, nanotechnology, as we know it in the 21st century, is gaining enormous acceptance in the electronic, manufacturing, agriculture, consumer-product, and food-additive industries as well as, more recently, the biotechnological and biomedical fields. Nanomaterials, such as titania (titanium dioxide) and silica (silicon dioxide, SiO_2), are used to improve and create new functional properties for common products (51). While nanomaterials based on biomaterials like polymers, such as poly (lactic-co-glycolic acid) (PGLA) or hydrogels, are considered of low toxicity, recent evidence has shown that some nanoparticles, such as metal, metal oxides (e.g., silica and titania), and carbon nanotubes, may pose potential risks to the environment, the food chain, and human health (35). Several studies have shown that nanoparticles can penetrate the body by different routes, including the skin, respiratory system, and gastrointestinal tract. In normal conditions, the inhalation of SiO_2 is likely the major route by which nanoparticles enter the body, and defective particle clearance in the airways increases the chance of particles translocating to different organs, including the heart, lungs, and kidneys (1, 45). Moreover, novel clinical diagnostic protocols and therapeutic drug treatments allow biological systems to undergo major and extended nano- and microparticle exposure, which can lead to an inflammatory response, fibrosis, oxidative stress, and cell death (15). Nano- and micro-SiO_2 particles have drawn a lot of attention in the biomedical field. Currently, different sizes of SiO_2 particles are being used in the clinical setting (23). Silica's usefulness as a biomedical tool has led to focused use in relation to human diagnostic, imaging, and labeling and in new targeting systems, which allows these nano- and micromaterials to interact directly with the body, leading to increased concentrations in the bloodstream and higher organ accumulation. In recent years, SiO_2 nano- and microparticles have been used extensively due to their chemical properties and

the capacity to manipulate their surface for different biomedical purposes, including for imaging and for therapeutic vehicles (5, 42, 50). However, while silicon-based particles have been considered to be of low toxicity and safe for use as a therapeutic vehicle (40), recent studies have shown evidence of toxicity, though this toxicity depends on a variety of factors, including the composition, differential toxicity among cell types, and—remarkably—particle size (13, 34, 38, 45). In particular, nanoscale particles (<100 nm) are a controversial topic of debate, and the related research conclusions lack consistency. For instance, *in vitro* and *in vivo* effects exerted by SiO_2 particles have recently been studied at the cardiovascular level, which showed cytotoxicity related to induced oxidative stress (10). Acute *in vivo* SiO_2 exposure also leads to an inflammatory response and endothelial dysfunction, which are strongly related to oxidative stress production and to impairments in myocardial antioxidant enzymes (8). Chronic exposure to SiO_2 particles has also been associated with alterations to different molecular mechanisms related to angiogenesis, heart formation and development, and pericardial edema and bradycardia, which can lead to cardiovascular diseases (10). More recently, microarray analysis showed that SiO_2 cardiotoxicity in a zebrafish model was related to oxidative stress and neutrophil-mediated cardiac inflammation (9). However, the mechanisms involved in SiO_2-induced toxicity in mammalian heart cells are still unknown.

In this study, we explored, for the first time, SiO_2-induced toxicity and impaired contractility and calcium handling in isolated adult cardiomyocytes exposed to 24 h incubation with two different sizes of SiO_2 particles: 7 nm AEROSIL® 380 Fumed Silica, which will be referred to henceforth as nano-SiO_2, and 670 nm particles synthesized by our group, which will be referred to henceforth as micro-SiO_2. We explored the mechanism of cell death caused by nano- and micro-SiO_2 at their half-maximal inhibitory concentration (IC_{50}) and related these effects to the phenomenon of SiO_2 particle association with

membrane and cellular uptake. Using confocal microscopy, we evaluated cardiomyocyte shortening and intracellular Ca^{2+} handling. In addition, we measured the mitochondrial membrane potential, oxidative stress, and ATP content to determine whether SiO_2 particles induced mitochondrial dysfunction and whether impairment of bioenergetics contributed to SiO_2-induced cardiac dysfunction.

Materials and methods

Chemicals

All reagents were obtained from Sigma-Aldrich (Sigma-Aldrich, St. Louis, MO) unless otherwise stated.

Synthesis of Micro-SiO_2

The 670nm SiO_2 particles were synthesized in accordance with the Stöber method (49). Briefly, a mix of 85 % of ethanol, 3.6 % of concentrated ammonium hydroxide solution and 11.5 % (v/v) of ultrapure water was stirred. Separately, a solution was prepared with 30.2 % of tetraethyl orthosilicate (TEOS), 13.2 % of (3-Aminopropyl) triethoxysilane (APTES) and 56.6 % (v/v) of ethanol. This second solution was added slowly to the first one and the mixture was magnetically stirred for 12 h. The resulting colloidal suspension was centrifuged and the precipitate was rinsed with pure ethanol, at least, three times. The solid was then dried in a muffle at 70 °C for 24 h. For the preparation of fluorescent silica spheres (F-Micro-SiO_2), dried Micro-SiO_2 spheres obtained of the aforementioned procedure, were subsequently calcined at 400 °C for 2 h. These calcined particles were then washed three times with ethanol in an ultrasonic bath. The fluorescence is attributed to the introduction of carbon and oxygen defects in the silica network after the calcination of APTES (20).

Nano-SiO_2 and Micro-SiO_2 characterization

Nano-SiO_2 (Degussa Co., Parsippany, NJ, US), Micro-SiO_2 and F-Micro-SiO_2 were characterized by a field-emission gun scanning electron microscope (FEG-SEM, model 200 Nova NanoSEM FEI Company).

The measurements were performed under low vacuum conditions, with a Helix detector and a 10-18 kV electron beam. Zeta potential and size measurements using dynamic light scattering (DLS) were performed on a Malvern Zetasizer Nano ZS90 (Malvern Instruments Ltd., Malvern, UK). Briefly, Nano- and Micro-SiO_2 were suspended in ultrapure water, Tyrode, M-199 and M-199 + bovine serum albumin (BSA) (5%) solutions and were irradiated with a red laser (HeNe laser, wavelength λ = 632.8 nm) and the intensity fluctuations of the scattered light (detected at a backscattering angle of 173°) were analyzed to obtain an autocorrelation function. The software (DTS v5.03) provided both the mean hydrodynamic diameter and polydispersity index, using the method of cumulants (according to the international standard ISO 13321:19963) and a size distribution using a regularization scheme by intensity, volume, and number. Crystalline structure was determined by X-ray diffraction (XRD) on a Panalytical Empyrean diffractometer (PANalytical Inc., Westborough MA, US).

Cardiomyocytes isolation

All the studies were performed in accordance with the animal care guidelines of the Guide for the Care and Use of Laboratory Animals published by the US National Institutes of Health (NIH Publication No. 85-23, revised 1996). All procedures were approved by the institutional animal use and care committee (protocol number 2011-Re-017). Rat ventricular myocytes were isolated by collagenase II digestion of perfused hearts (14). Briefly, male Wistar rats weighing 250-300 g were used to isolate cardiac cells. Animals were heparinized and anesthetized with pentobarbital (1000 U/kg and 100 mg/kg, i.p. respectively) before removal and hanging the heart. Hearts were mounted on a Langendorff apparatus and then perfused with Tyrode medium (TM), in mM: 128 NaCl, 0.4 NaH_2PO_4, 6 glucose, 5.4 KCl, 0.5 MgCl-$6H_2O$, 5 creatinine, 5 taurine and 25 HEPES, pH 7.4 at 37 ºC., for 5 min and digested by 0.1% collagenase type II (Worthington Biochemical, Lakewood, NJ) dissolved in TM for 15 min. Ventricles

were dissected and cells mechanically disaggregated. Cardiomyocytes were washed in crescent concentrations of calcium (0.25, 0.5, 1 and 1.5 mM) plus 0.1% albumin contained in the TM. Intact cardiomyocytes were cultured in M-199 medium supplemented with (in mM): 5 taurine, 5 creatine, 2 L-carnitine, 2.5 sodium pyruvate, penicillin (100 U/ml) and streptomycin (100 µg/ml) on a laminin-coated culture dishes at a density of 1 x 10^4 viable cells per cm^2. Cells were incubated at 37 °C in 95 % air and 5 % CO_2 for 2 h prior to all experiments.

Determination of Nano-SiO_2 and Micro-SiO_2 cytotoxicity and cell death mechanisms

To determine SiO_2 cytotoxicity, varying concentrations of Nano- and Micro-SiO_2, were added to culture media and the incubation was continued for 24 hours. At the end of the incubation period, cytotoxicity of SiO_2 was determined using the Alamar Blue viability test (Life Technologies, Carslbad, CA, US). The IC_{50} was calculated using Origin software (Northampton, MA, US). Necrosis and apoptosis were measured with Ghost Dye Red 780 and Annexin V-PE-Cy7- stained cells using a BD FACSCantoII flow cytometer (BD Biosciences, Heidelberg, Germany). Cells were stained according to the manufacturer's instructions. Briefly 1 uL of Ghost Dye (Tonbo Bioscience, San Diego, CA) solution was added in 1 mL of TM and incubate for 30 min, washed and resuspended in 300 uL with 5 µL of fluorochrome-conjugated Annexin-V-PE-Cy7 (eBioscience, San Diego, CA) by 10 min at room temperature. Finally cells were washed and fixed using 4% paraformaldehyde by 20 min. Following incubation; cell monolayers were washed twice with TM and detached from the culture plate by scrapping. In total 10,000 cells were analyzed per measurement in TM solution and data was analyzed using FlowJo 8.8.6 software (Treestar Inc, Ashland, US). The release of cytoplasmic lactate dehydrogenase (LDH), as a marker of cell integrity and necrosis, was determined enzymatically followed the interconversion of pyruvate and lactate and with concomitant oxidation of NADH to NAD^+ followed by using spectrophotometry at 340 nm. Values

were adjusted to an LDH calibration curve. The activity of caspases 3 and 7, to assess SiO_2-induced apoptosis, was measured in cell pellets using the Apo-ONE fluorescent substrate (Promega, Madison, WI, USA).

Characterization of Nano-SiO_2 and Micro-SiO_2 in the cardiomyocyte

In order to assess the interaction between cardiomyocytes membrane and SiO_2 particles, a 24 hours cell incubation with Nano- and Micro-SiO_2 was analyzed by FEG-SEM. Samples were prepared by seeding cardiomyocytes on to 5×7 mm silicon chips specimen supports (Ted Pella, Redding, CA, USA). Samples were fixed with 2.5 % glutaraldehyde, in PBS buffer (Electron Microscopy Sciences, Hatfield, PA, USA) for 20 min, then dehydrated in increasing concentrations of ethanol for 10 min. Specimens were mounted on SEM stubs (Ted Pella, Redding, CA, USA) using conductive adhesive tape (Ted Pella, Redding, CA, USA) and coated with a gold thin film. FEG-SEM surface images were acquired at different magnifications under high vacuum, at 15.00 kV, spot size 3.0, using a Nova NanoSEM 200 (FEI, Hillsboro, OR, US). The energy-dispersive X-ray spectroscopy (EDS) analysis was performed with an Oxford Instruments analyzer and was performed at 15 kV. In addition to surface images, transversal cuts were done on random cardiomyocytes by Focused Ion Beam, and EDS was performed to assess the intracellular location of the SiO_2 particles using a Zeiss Crossbeam 340, using 30kV for the FIB and 12 kV for the SEM. Ten individual cells from each treatment were selected randomly for imaging and EDS analysis.

Particle-induced X-ray emission (PIXE) was used to quantify the total amount of silica present in the cardiomyocytes. This technique has been used recently for nanomaterial quantification in complex matrices (25). A 2.5 MeV proton beam was used to irradiate the cells with currents < 1 nA to reduce sample damage. The cardiomyocytes were incubated with Nano- and Micro-SiO_2 at its IC_{50} with

different end time points (0, 1, 12 and 24 h). After each incubation time, cells were: 1) washed with M-199 to remove free particles, 2) detached from the culture plate and 3) centrifuged at 500 rpm through a 250 mM sucrose solution to separate non-internalized and non-adhered silica particles as well as dead cardiomyocytes from the intact cells. The pellet (alive cells) was resuspended in 200 µL of MilliQ H_2O, finally transported sequentially into truncated sample holders and removing the aqueous media following as previously reported (26). Data analysis was done with the GUPIXWIN software (7).

Intracellular localization of F-Micro-SiO_2 by confocal microscopy examination

To determine the intracellular localization of F-Micro-SiO_2, cardiomyocytes were seeded into laminin-covered glass coverslips. Cells were incubated with F-Micro-SiO_2 for 24 hours, followed by fixation and staining of cellular structures. Briefly, after SiO_2 incubation, cells were fixed using 4% paraformaldehyde in PBS buffer for 20 min. Immunofluorescence staining was performed by cell permeabilization with 0.1% Triton-X 100 (Thermo Fisher Scientific, Waltham, MA, US) in PBS for 3 min. Cells were rinsed three times in PBS and a blocking step with 1 % bovine serum in PBS was performed for 10 min. Actin filaments were stained with 0.5 unit/µl of Alexa Fluor 568-conjugated phalloidin (Life Technologies, Grand Island, NY, USA) for 20 min at room temperature. Glass coverslips were rinsed with PBS and mounted using vectashield mounting media (Vector laboratories, Burlingame, CA, USA). Samples were imaged using a Leica TCS SP5 confocal microscope equipped with a D-apochromatic 63X, 1.2 NA, oil objective (Leica Microsystems, Wetzlar, Germany). To assess cellular internalization of F-Micro-SiO_2, a stack of 2D images, with a focal plane thickness of 1 µm, were collected every 1 µm along z-axis using an excitation (*ex*) and emission (*em*) of 488 nm and 500-700 nm respectively. For the representative images to assess cellular internalization of F-Micro-SiO_2, wavelengths of an *ex* of 488 nm and 543 nm, and *em* of 500-600 nm and 620-720 nm, for F-Micro-SiO_2 and cytoskeleton were used

respectively. The tridimensional reconstructions were made from z-stacks with a focal plane thickness of 2 µm, using the 3D viewer plugin from ImageJ (NIH, Bethesda, US).

Ca^{2+} handling and cell shortening in intact cardiomyocytes

The Ca^{2+} transients, Ca^{2+} sparks, and cell shortening parameters were measured as previously described (29, 53). 24 hours cultured cardiomyocytes on laminin-covered glass coverslips, with Nano- and Micro-SiO_2 at its IC_{50}, were incubated in TM with Fluo-4 AM or Fluo-3 AM (Life Technologies, Carlsbad, CA, US) to evaluate Ca^{2+} handling, and cell shortening. Afterwards, the cells were washed with a fluorophore-free solution. Loaded cells were mounted in a superfusion chamber. All fluorescence measurements were acquired with a Leica TCS SP5 confocal microscope equipped with a D-apochromatic 63X, 1.2 NA, oil objective (Leica Microsystems, Wetzlar, Germany). Line scan images were recorded along the longitudinal axis of the cell at 400 Hz using an Argon laser to excite the fluorophore at 488 nm and its emission was collected at 500-600 nm. For cell shortening, a pinhole optimized for a 4 µm section thickness in the focal plane was used, while a 1 µm section thickness was used for Ca^{2+} signaling. Cell shortening was evaluated under field stimulation at 0.5, 1 and 2 Hz (MYP100 MyoPacer Field Stimulator; Ion-Optix, Milton, MA). For Ca^{2+} transient and Ca^{2+} sparks the cells were field stimulated by 3 to 5 electric pulses at 1 Hz to attain steady state sarcoplasmic reticulum (SR) Ca^{2+} content. The Ca^{2+} signaling under β-adrenergic stimulation was evaluated by perfusion of isoprenaline (ISO) at 100 nM and the records were taken after 10 min of exposition. For SR Ca^{2+} content, the cells were field stimulated at 1 Hz before a rapid caffeine application at 10 mM. Fluorescence data were normalized as $\Delta F/F_0$, where F is fluorescence intensity and F_0 is average fluorescence at rest.

Bioenergetic status measurements

Mitochondrial membrane potential (Δψ) was evaluated in cultured cardiomyocytes by confocal microscopy using a Leica TCS SP5 confocal microscope equipped with a D-apochromatic 63X, 1.2 NA, oil objective (Leica Microsystems, Wetzlar, Germany). Cardiomyocytes on laminin-coated coverslips were treated with Nano-SiO_2 for 24 hours, washed with TM to remove particles and loaded with 300 nM tetramethylrhodamine ethyl ester perchlorate (TMRE, Thermo Fisher Scientific, Waltham, MA, US) during 30 minutes at room temperature and darkness. TMRE accumulates in metabolically active mitochondria producing a fluorescence that is proportional to Δψ (44). Afterward, the cells were rinsed with fluorophore-free TM and placed in a recording chamber. TMRE signal was measured with an *ex* at 543 nm and an *em* to 560-700 using oil immersion 40X objective. To evaluate the Δψ, records were taken after field stimulation at 1 Hz. The 2-dimensional images were acquired with Leica LAS AF version 2.7 format at 400 Hz with 512 x 512 image size and a focal plane thickness of 1 µm. The total fluorescence from the 2-D images was evaluated and plotted as a percentage of relative fluorescence, being control group the 100%. ATP content was measured in control group (CT) cardiomyocytes as well as those treated with Nano-SiO_2 at its IC_{50}, after a 24 h exposure, using the CellTiter-Glo Luminescent Assay (Promega. Madison, US).

Oxidative stress markers

A change in the concentration of H_2O_2 in the medium was detected by fluorescence of the oxidized Amplex Red (Life Technologies, Carlsbad, CA, US) using wavelengths of *ex* at 550 nm and *em* at 585 nm. The response of Amplex Red to H_2O_2 was calibrated by sequential additions of known amounts of H_2O_2 from 100 to 1000 pmol/min. Glutathione (GSH) was measured as previously described (39). Briefly, cells were dissolved in medium containing (in mM): 50 KH_2PO_4, pH 7.5 with the addition of 0.2% Tx-100, 1 PMSF and 0.6 % sulfosalicylic acid for 10 min a 4 °C and centrifuged at 8000 rpm for 10 min.

Protein concentration was measured by Lowry method. 30 μg of protein were incubated in a medium that contained (in mM): 50 KH_2PO_4, 1 EDTA, pH 7.5 with the addition of GSH reductase 10 U/ml, 0.1 DTNB and 2 NADPH. The reduction of DTNB was followed at 412 nm and quantified with extinction coefficient (13.6 $M^{-1}cm^{-1}$).

Statistical analyses

Data were analyzed by ANOVA followed by Dunnett's multiple comparisons tests using Graph Pad InStat (Graph Pad Software Inc., San Diego, US) or by student t-test, as indicate. Data were expressed as mean ± S.E.M. A p-value <0.05 was considered statistically significant.

Results

Characterization of SiO_2 particles

The characterizations of the nano- and micro-SiO_2 particles are presented in Figure 1. The field-emission gun scanning electron microscope (FEG-SEM) images show that the micro-SiO_2 had a spherical shape and exhibited dispersibility (Figure 1A). The size distribution shown by FEG-SEM analysis had an average diameter of 670 ± 32 nm (insert, Figure 1A), while the average diameter of nano-SiO_2 was 7 nm according to the manufacturer's technical sheet. Analysis of the crystalline structure using XRD showed that the nano- and micro-SiO_2 particles presented an amorphous structure (Figure 1B). The hydrodynamic diameters (Figure 1C) of the nano- and micro-SiO_2 particles in ultrapure water were 91 ± 22 nm and 712 ± 212 nm, respectively. The zeta potentials of the nano- and micro-SiO_2 particles (Figure 1D) were -27.1 ± 4.4 mV and -14.4 ± 5.48 mV, respectively. Hydrodynamic diameters and zeta potentials were also measured in Tyrode, M-199, and M-199 + BSA solutions (Table 1). In addition, EDS analysis showed that the purity of the silica particles was higher than 95%, and no

traces of other metals were detected in the particle suspensions (data not shown).

Dose- and time-dependent cytotoxicity of nano- and micro-SiO_2 particles

To assess the effects of SiO_2 on cardiomyocyte viability, adult-rat ventricular myocytes were cultured with different concentrations of nano- and micro-SiO_2 particles, and cell death was examined after 24 h of treatment. As shown in Figure 2A, nano- and micro-SiO_2 induced significant cytotoxic effects in a dose-dependent manner, with IC_{50} values of 99.5 ± 12.4 μg/ml and >1500 μg/ml, respectively, which indicates that nano-SiO_2 has a15-fold higher toxicity than micro-SiO_2. Indeed, when the cardiomyocytes were cultured in the presence of nano- and micro-SiO_2 at the IC_{50} of nano-SiO_2, only nano-SiO_2-induced cell death occurred as a result of the necrotic pathway. No evidence of apoptosis was observed in any case, as shown by the lack of single positive Annexin V cells (Figure 2B-C) and the lack of caspase 3/7 activity (data not shown). In addition, necrosis induction also occurred faster with nano-SiO_2 than with micro-SiO_2 as shown in Figure 2D by the lactate dehydrogenase (LDH) leakage. Nano-SiO_2 promoted cardiomyocyte necrosis in the first 3 h of incubation, while micro-SiO_2 only led to significant LDH leakage after 12 h at their corresponding IC_{50} values.

SiO_2 particles associate with the cellular membrane and internalize in the cell

In order to relate cellular death to particle membrane association or to the potential internalization of the SiO_2 particles, we analyzed the association of single or agglomerates/aggregates of nano- and micro-SiO_2 to the cardiomyocytes' cellular membranes, as shown in Figure 3A-B. The FEG-SEM images show the association of the SiO_2 particles with the cell membrane 24 h after administration in the cultured adult-rat cardiomyocytes at 37°C (Figure 3A-B). Figure 4 depicts the surface of the cardiomyocytes using EDS, which shows that the nano- and micro-SiO_2 particles have individual and

agglomerate/aggregate associations with the cellular membrane with respect to the four EDS images of the elemental maps for carbon, sodium, silicon, and oxygen. Transversal cuts in the cardiomyocytes with nano- or micro-SiO_2 (Figure 3C-E) showed that the particles could internalize in the cardiomyocytes after 24 h incubation. Figure 3F shows the SiO_2 content quantified by particle-induced X-ray emission (PIXE) in the cardiomyocytes as a function of time. A time-dependent increase was observed in SiO_2 in the cardiomyocytes treated with nano- and micro-SiO_2 particles, suggesting an association/internalization of the silica particles in the cardiomyocytes. Furthermore, EDS analysis in the transversal cut in the cardiomyocytes indicates that the SiO_2 signal is higher in nano-SiO_2 versus micro-SiO_2 particles, which suggests that smaller SiO_2 particles are more prone to cellular internalization in cardiomyocytes. As shown in Figure 3G, we explored, by confocal microscopy, the internalization of micro-SiO_2 after 24 h incubation, and we analyzed the confocal z-stack acquisitions. For this purpose, we synthesized a micro-SiO_2 particle with fluorescent properties (F-micro-SiO_2) that had a similar size, morphology, dispensability, and zeta potential as micro-SiO_2 (Table 1). Using this approach, we confirmed the presence of multiple single and agglomerate/aggregate F-micro-SiO_2 at different subcellular levels using a tridimensional reconstruction captured from cardiomyocytes, thereby confirming the intracellular localization of SiO_2 particles (Figure 3G, Video 1). We also visualized the internalization of the F-micro-SiO_2 through confocal z-stack analysis, which confirmed the presence of particles (shown as bright spheres) near the nuclei area (shown as dark ovals) (Figure 3G). Figure 5 shows a semi-quantitative analysis wherein the total fluorescence in a z-stack was evaluated to determine the internalization of the F-micro-SiO_2 in intact cardiomyocytes exposed to different concentrations of particles during 24 h incubation. F-micro-SiO_2 exhibited dose-dependence at low concentrations (Figure 5A) and was able to reach a saturating concentration without promoting

significant cellular death (data not shown), which is similar to micro-SiO_2 at the same concentration (Figure 2A), and we showed that cardiomyocytes treated with 150 μg/ml of F-micro-SiO_2 preserved their normal morphology (Figure 5B). At the maximum evaluated concentration of 150 μg/ml, we observed a two-fold increase in fluorescence; the 1 ± 0.17–fold fluorescence presented in the untreated (CT) group increased to 2.02 ± 0.41–fold in the F-micro-SiO_2-treated group (Figure 5B).

SiO_2 treatment induced a reduction in cell shortening, decreased SERCA activity, and impaired β-adrenergic stimulation

Cardiomyocyte sarcomere shortening (Figure 6) following nano- and micro-SiO_2 treatment reduced by 34% and 36%, respectively, compared to the CT group. This impairment in cell shortening was maintained at 0.5 and 2 Hz. However, no difference was evident between the nano- and micro-SiO_2 groups. For the purpose of exploring the mechanism of this impairment, we chose to work with nano-SiO_2 particles at 100 μg/ml in order to match the physiological conditions of airways and to avoid high range concentrations (IC_{50} values of >1500 μg/ml for micro-SiO_2) that could not be detected *in vivo* after a short exposure.

Generally, the changes in cardiomyocyte Ca^{2+} handling followed the time course of the changes in contractility. In this sense, Figure 7A-B shows a representative recording of Ca^{2+} transients evoked by field stimulation for the control and nano-SiO_2-treated cells. Figure 7C shows the pooled data of the change in the Ca^{2+} transient peak amplitude upon physiological β-adrenergic stimulation ISO in both cell treatments. We found that under basal conditions, the peak Ca^{2+} transient amplitude was similar in the SiO_2-treated and CT cells (6.03 ± 0.27 $\Delta F/F_0$ CT *vs*. 6.72 ± 0.37 $\Delta F/F_0$ nano-SiO_2). However, after 10

min of continuous β-adrenergic stimulation, the Ca^{2+} transient amplitude increased to only 7.95 ± 0.72 in the nano-SiO_2-treated cells, while the control group increased to 9.13 ± 0.59 ($P < 0.05$).

For relaxation, the released Ca^{2+} must be removed from the cytosol; SERCA and the sarcolemmal Na^+/Ca^{2+} exchanger perform this activity. In this context, the Ca^{2+} transient time to 50% decay ($T_{50\%}$) provides an index of the combined activity of the Ca^{2+} removal systems; however, the SERCA activity underlies more than 90% of Ca^{2+} removal (4). Figure 7D shows the Ca^{2+} transient $T_{50\%}$ plotted under basal conditions and as a function of time during ISO perfusion. Under basal conditions, the $T_{50\%}$ of the nano-SiO_2-treated cells was 331 ± 23 ms, while that of the CT cells was 239 ± 11 ms ($P < 0.05$). In both cases, there was an increase in the cytosolic Ca^{2+} removal rate after adrenergic stimulation; however, there was still a difference between the CT and nano-SiO_2-treated cells (183 ± 7 and 233 ± 14 ms, respectively; $P < 0.05$). This result suggests impairment in SERCA activity.

Because alterations in Ca^{2+} handling in other pathological settings are also reflected at the level of diastolic Ca^{2+}, we measured whether the spontaneous Ca^{2+} sparks were altered in the SiO_2-treated cardiomyocytes. Figure 8A shows the typical Ca^{2+} spark reconstruction in the CT (left) and nano-SiO_2-treated cardiomyocytes (right). Calcium spark analysis revealed a significant decrease in frequency in the nano-SiO_2 group (1.81 ± 0.28 sparks/100 µm/sec nano-SiO_2) compared with the CT group (2.79 ± 0.26 sparks/100 µm/sec CT) ($P < 0.05$) (Figure 8B) and a significant decrease in amplitude (0.82±0.02 F/F_0 CT *vs.* 0.65±0.03 F/F_0 nano-SiO_2; $P < 0.05$) (Figure 8C), which might indicate reduced SR calcium content. We estimated a steady-state SR Ca^{2+} content by the cytosolic peak of the caffeine-evoked Ca^{2+} release in the CT and SiO_2-treated cells. Figures 9A-B shows representative confocal images of caffeine-evoked SR Ca^{2+} release in the control and nano-SiO_2 treated cells, respectively. Pooled data of the peak

caffeine-evoked Ca^{2+} release is shown in Figure 9C. The nano-SiO_2 cells had a slightly lower SR Ca^{2+} content, the difference was not statistically significant under basal conditions (5.48 ± 0.35 and 4.59 ± 0.46 for CT and nano-SiO_2 treated cells, respectively; $P < 0.12$).

SiO_2 treatment induces a decrease in mitochondrial membrane potential and ATP content

Efficient Ca^{2+} handling, which is necessary for proper contraction and relaxation, depends strongly on the ATP supply in the vicinity of SERCA (11). In this regard, we explored whether SiO_2 treatment affected the bioenergetics status in nano-SiO_2-treated cardiomyocytes (Figure 10 A-B). Figure 10C shows a 29.5% decrease in the mitochondrial membrane potential ($\Delta\psi$) with nano-SiO_2 treatment compared to the CT group after 24 h incubation. This finding was strongly related to the ATP content in the cardiomyocytes, as nano-SiO_2 treatment reduced the ATP content by 60% compared to the CT cells (Figure 10D). These findings suggest that the SiO_2 particles impaired mitochondrial function.

SiO_2 induces ROS production and glutathione depletion

Modification of the redox state by nano- and microparticles has been reported as one of the main mechanisms of cytotoxicity at the cellular level (35). In this regard, we incubated cardiomyocytes with nano-SiO_2 for 24 h and then measured H_2O_2 production and glutathione (GSH) content. Figure 10E shows that the SiO_2 particles significantly increased H_2O_2 production and markedly depleted GSH (Figure 10F) compared to the CT group. Nano-SiO_2 induced a significant reduction in GSH (down to 6.5 nmol/mg) in comparison to the CT group (15.4 nmol/mg), which shows that silica particles exerted a pro-oxidative status on adult-rat cardiomyocytes.

Discussion

The purpose of this study was to evaluate, for the first time, the potential cardiotoxicity of SiO_2 particles in adult cardiomyocytes and their effects on excitation–contraction coupling. In addition, recent results have shown that silicon-based microparticles associate and accumulate in a failing myocardium (in contrast to a healthy myocardium) following intravenous administration, and the microparticles reach the cardiomyocytes. This finding points to a novel avenue for developing nanotechnology-based therapeutics and diagnostics for heart failure and other cardiomyopathies that involve endothelial dysfunction and a proinflammatory milieu (40). In addition, there is great interest in using these materials therapeutically as vehicles for carrying genes, siRNA, drugs, or peptides, and there are promising results (5, 42) due to their physicochemical properties, the capacity of biochemical functionality and surface modification to immobilize biomolecules, and the easy preparation of diverse particle sizes (nano and micro) with uniform shapes and structures (37).

SiO_2 nanoparticle internalization is associated with cardiotoxicity

SiO_2 particles have displayed various cytotoxic effects at the cellular level, which has led to growing concern about their safety (15, 33, 35). Importantly, the toxicity of SiO_2 particles might depend on their crystalline nature and morphology, but this was not considered as a variable in this work because nano- and micro-SiO_2 have a spherical shape and the same crystalline nature. However, one important factor for consideration in this work is the particle size (45). It is generally accepted that the smaller the particles, the greater the toxicity exerted in biological systems. In our study, we found differential cardiotoxicity between nano- and micro-SiO_2. In agreement with many previous studies (34), nano-SiO_2 particles exerted potent cytotoxicity compared with micro-SiO_2 particles at the same concentration (e.g., 300 μg/ml). Nano-SiO_2 reduced viability nearly 80%, as compared to 30% for micro-SiO_2. Our

414 results indicate that nanoparticles are more toxic to adult-rat ventricular myocytes than microparticles.
415 Consistent with our results, Duan et al. (9), using 70 nm SiO_2 nanoparticles, observed pericardial edema
416 and cardiac toxicity in zebrafish embryos, which affected heart rhythm. These observations should be
417 considered when designing new products for medical applications or for novel vehicles for gene/drug
418 delivery.

419 We previously mentioned our decision to evaluate SiO_2 particle size and stability in ultrapure water
420 and, more importantly, in culture media (Tyrode, M-199, and M-199 + BSA) in order to know SiO_2
421 particle properties where all experiments have been performed. One of the main characteristics of the
422 DLS technique is that DLS "is a function of the relative refractive indices of the particle or molecule and
423 the dispersant" (24). In our case, when measurements are made in a culture medium, the molecules
424 within it scatter light, which causes interference; thus, the data can probably not be gathered with
425 100% efficiency. However, the changes in the physicochemical properties (particle size distribution and
426 surface charge) of the SiO_2 particles in the culture media were determined using an incubation
427 protocol adapted from Monopoli et al. (32) to assess the formation of the hard protein corona around
428 the particles. The results, as shown in Table 1, effectively indicate that the more complex the media in
429 which the SiO_2 particles are exposed, the greater the tendency to increase in size; nevertheless, we
430 showed that their surface charge remained relatively unmodified, as it remained negative for all
431 samples under all tested conditions. The zeta potential of the nano-SiO_2 was -24.1 mV, while for the
432 micro-SiO_2 and its fluorescence-modified counterpart it was -14.4 and -33.6 mV, respectively. Overall,
433 these changes are not significant enough to expect dramatic changes in their interaction with cells,
434 such as in the internalization effects. It was not until relatively recently that the ζ-potential, which
435 represents the surface charge of a given set of particles, became relevant as a key factor that

436 influences processes such as opsonization and internalization. Examples of such dramatic changes were
437 presented by Arvizo et al. (2), who tested these aforementioned key factors in gold nanoparticle–
438 coated polymers that conferred surface charges that were positive, negative, or neutral. They found
439 that particles with a neutral surface charge (i.e., a zeta potential < |2| mV) had longer circulation times
440 and consequently higher accumulation in tumors. Other studies with cancer cell lines, such as HeLa (18,
441 30), and endothelial cells (43) found *in vivo* that particles with a positive surface charge had higher
442 internalization rates than negative or neutral particles. For cardiac cells specifically, Miragoli et al. (31)
443 found that exposure in cultured neonatal-rat myocytes to 50 nm-charged polystyrene particles showed
444 contrasting effects based on the type of surface charge: positively charged particles showed higher
445 cytotoxic effects, while negatively charged particles showed lower cytotoxicity but formed 50–250 nm
446 nanopores that induced pro-arrhythmic events.

447 In this work, we observed differences in the cell-release levels of LDH after 24 h incubation of SiO_2. As
448 shown in Figure 2C, nano-SiO_2 produced a two-fold increase in activity compared with micro-SiO_2-
449 treated cells. This difference was made more evident by the fact that SiO_2-induced necrosis occurred in
450 a time-dependent manner, in accordance with previous reports, and nano-SiO_2 caused LDH leakage in
451 endothelial cells at similar times and doses (10). Figure 2D shows cell-membrane damage as early as in
452 the first three hours of incubation with nano-SiO_2; this phenomenon is probably due to the size of
453 nano-SiO_2, which allows it to penetrate faster through the cell membrane, in turn causing an early
454 permeabilization process that has important cytotoxic effects. This cytotoxic effect was also exerted by
455 the micro-SiO_2 as early as the first two hours, but significant LDH release was shown only after 12
456 hours of incubation. In this scenario, membrane permeabilization and LDH release indicate the

beginning of necrosis in SiO_2-treated cells. Apoptosis cell death was not observed, potentially due to the reduced energetic metabolites.

As observed, micro-SiO_2 exerted a lower cytotoxic effect compared with nano-SiO_2. To understand this difference, we developed a hypothesis with two scenarios: 1) micro-SiO_2 does not associate properly with cardiomyocyte membranes, and 2) the larger particle size of micro-SiO_2 prevents it from penetrating into cardiomyocytes, thus avoiding membrane disruption and cell damage. Based on this, we explored the association of SiO_2 particles with cellular membranes. The FEG-SEM micrographs show that nano- and micro-SiO_2 associated with cells as individuals and agglomerates/aggregates, and there was evidence of an internalization process and a strong interaction between SiO_2 and cell membranes. In accordance with this, the quantification by PIXE revealed that there was a concentration of SiO_2 in the cardiomyocytes,, while no traces of SiO_2 were found in the unexposed cells (CT group). The concentration increased 3.3- and 4.5-fold for nano- and micro-SiO_2, respectively. These concentrations correspond to particles that were either internalized or that adhered to the cardiomyocytes.

To explore the second hypothesis, we incubated fluorescent micro-SiO_2 and analyzed its internalization using confocal microscopy. We confirmed that micro-SiO_2 was localized inside the cardiomyocytes, following a dose-dependent manner, with some association near the nucleus, an interesting phenomenon that is widely observed in different phagocytic cellular types (13, 27) but rarely explored in non-dividing cells. Adult cardiomyocytes, as a non-dividing cell type and with an apparent non-phagocytic capacity, represent an interesting opportunity to study the biological phenomena of nano- and microparticle internalization and intracellular trafficking. Our group recently studied the

mechanisms for the internalization, trafficking, and perinuclear particle localization of these-apparently not-quiescent cardiomyocytes (40).

Calcium mishandling is associated with SiO_2 nanoparticle cardiotoxicity

Aberrant Ca^{2+} handling is an important contributor to the electrical and contractile dysfunction associated with cell death. Recently, Gilardino et al. (16) found evidence that, in a neuronal cell line, SiO_2 nanoparticles induce oscillatory changes in intracellular Ca^{2+}. Although Ca^{2+} returns to baseline in about 4 h, these authors suggests that several voltage-dependent Ca^{2+} channels on the plasmatic membrane are responsible for these effects. Our results do not agree with this, as they suggest that extracellular Ca^{2+} transport remains functional between the L-type Ca^{2+} channel and SR interaction because the time to peak of Ca^{2+} release remains intact (data not shown). On the other hand, we observed that the decreased contractility in SiO_2-treated cardiomyocytes could also be due to alterations in Ca^{2+} signaling. In this regard, we found that the electrically evoked Ca^{2+} transients were blunted with slow decay and were less sensitive to physiological β-adrenergic stimulation during ISO perfusion. The reduced Ca^{2+} transient amplitude could be due to either decreased SR Ca^{2+} content or a decrease in the L-type Ca^{2+} channel current density. The general consensus is that there is a modest change, or no change, in the Ca^{2+} current, even in the context of pathologies as profound as heart failure. However, there is much evidence associated with a state of SR Ca^{2+} depletion in pathologies such as doxorubicin-induced cardiomyopathy (36). Decreased SERCA activity and lower intra-SR Ca^{2+} content in SiO_2-treated cardiomyocytes might explain the smaller amplitude of Ca^{2+} transients and Ca^{2+} sparks. The lower SR Ca^{2+} content in SiO_2 nanoparticle–treated cells, as well as the slow rate of Ca^{2+} transient decay, could be explained by different events that can alter the SERCA function, such as low ATP content, as shown in this work (Figure 10), or a decreased SERCA expression, which was recently

observed in microarrays from zebrafish embryos treated with SiO_2 nanoparticles (9). However, several studies have shown that decreased SERCA activity is not necessarily accompanied by decreased protein expression (55), and it has been pointed out by our group that Ca^{2+} signaling alterations may precede the changes in protein expression (24). To explain diminished capacity of SERCA to reload the SR, we should consider the consequences of mitochondrial dysfunction due to the drop in membrane potential and the low ATP content (Figure 10), particularly during high cardiac workloads. A reduced capacity for energy supply (22) and the ineffective removal of the end products of ATP hydrolysis have been observed in heart failure, which leads to a reduction in the phosphorylation potential, which can in turn affect the ATPases involved in Ca^{2+} handling (22). SERCA is one of the most energy-demanding, and therefore most sensitive, cardiac enzymes in ATP depletion. Based on this, dysfunctional mitochondria and a lower ATP content could undermine cytosolic Ca^{2+} removal by SERCA, decrease contractile strength, and slow muscle relaxation, which we observed in SiO_2-treated cardiomyocytes. However, while the SR Ca^{2+} content was slightly lower in the SiO_2-treated cells, under basal conditions we found a decrease in the spontaneous Ca^{2+} spark amplitude and frequency. Because a steady state SR Ca^{2+} content results from the balance between SERCA activity and SR Ca^{2+} leakage, the latter reflected spontaneous Ca^{2+} sparks and the decrease in SR Ca^{2+} leakage might explain the lower SR Ca^{2+} content observed in cells treated with SiO_2 nanoparticles; this phenomenon could also be exacerbated and deregulated under continuous β-adrenergic stimulation, as we showed in our electrically evoked Ca^{2+} transients under ISO stimulation (Figure 7). Altogether, these findings are in agreement with reports on ventricular dysfunction and ischemic heart disease in which diastolic Ca^{2+} release is increased (12, 53).

Mitochondrial dysfunction as a trigger of SiO_2 toxicity

As we mentioned before, in cardiomyocytes the excitation–contraction coupling and metabolic adaptations are based on the coordination between the mitochondria and SR, which facilitates the ATP supply for SERCA activity and ensures energy replenishment by Ca^{2+} and ADP exchange (14, 52). For this reason, mitochondrial function is recognized as an important player in regulatory Ca^{2+} signaling in the heart (52). However, the impact of SiO_2 nanoparticles on energy metabolism and mitochondrial function is largely unclear. Our findings demonstrate that exposing cardiomyocytes directly to SiO_2 nanoparticles for 24 h induced mitochondrial membrane depolarization and energy debacle (Figure 10), and even more membrane depolarization and energy debacle after 10 min of continuous β-adrenergic stimulation under ISO treatment (data not shown).

Xue et al. (54) observed SiO_2 nanoparticle–induced suppression of mitochondrial dehydrogenase activity and ATP synthesis in hepatocytes. Following *in vitro* exposure, the internalization of SiO_2 nanoparticles correlates with the disturbance of the mitochondrial structure and the release of reactive oxygen species (ROS) in hepatocellular carcinoma cells (47). In this context, cardiac mitochondria allow energy supply–demand matching and regulate the generation of antioxidant defenses, such as nicotinamide adenine dinucleotide phosphate and GSH (28). However, under the Ca^{2+} handling impairment—as observed during SiO_2 nanoparticle interaction—increased electron leakage from the electron transport chain, and the subsequent production of ROS and depletion of antioxidant reserves, has been observed (19). Similar to previous results, it was observed that nano-SiO_2 incubation induced a significant amount of H_2O_2 (a highly toxic type of oxygen-free radical) and a potent depletion in GSH (a first-line antioxidant defense), which indicates SiO_2-induced cytotoxicity that is at least partially due to an imbalance in the cellular redox status. In this regard, it is possible that SERCA and/or the ryanodine receptor might be oxidized, as has been described in other works (3), and

543 this could, at least partially, underlie the slow rate of Ca^{2+} transient decay and the decrease in the
544 amplitude and frequency of sparks. An enhanced diastolic Ca^{2+} leak may not only contribute to the
545 decreased SR Ca^{2+} content but also increase the risk of delay after depolarization and Ca^{2+}-triggered
546 arrhythmias, as previously observed by Szebeni et al. (48) with lipid-based nanoparticles in a pig model.
547 A recent study also showed another possible mechanism of cardiotoxicity with metal-oxide
548 nanoparticles. Savi et al. (41), using nano-TiO_2 particles that had a z-potential similar to that of our
549 nano-SiO_2 particles but a different crystalline nature (a mixture of anatase and rutile, as compared to
550 our amorphous SiO_2), observed that nano-TiO_2 particles promoted spontaneous contraction in
551 cardiomyocytes (an arrhythmia trigger at the cellular level). This effect was related to the slight
552 depolarization of the resting membrane potential, which consequently reduced the action potential
553 duration. Then, using an in silico model, they suggested that nano-TiO_2 particles generate transient
554 nanopores that lead to resting membrane potential instability, possibly due to K^+ leakage (41).
555 In this context, our results with nano-SiO_2 particles suggest that there was no change in the action
556 potential because the kinetics of Ca^{2+} release from the sarcoplasmic reticulum were not affected (time
557 to peak; data not shown) and spontaneous contraction was not observed. However, our experiments
558 were performed at 24 h, while the TiO_2 particles were analyzed 1 h after particle addition, so further
559 experiments on patch-clamped cardiomyocytes with simultaneous measurement of Ca^{2+} handling
560 might help to establish a potential connection between these mechanisms of cardiotoxicity.
561 Interestingly, the nano-TiO_2 particles induced lipid peroxidation in the heart due to ROS production,
562 which is similar to our findings regarding GSH and H_2O_2 levels.
563 Putting all of this information into context, as summarized in Figure 11, the Krebs cycle generates the
564 NADH required for oxidative phosphorylation through the electron transport chain (complex I-IV, in

565 blue). This step-by-step transfer of electrons allows protons from the mitochondrial matrix to be
566 transported uphill across the inner mitochondrial membrane, which forms a proton concentration
567 gradient ($\Delta\Psi_m$). Thus, free energy released during the oxidation of NADH is stored both as an electric
568 potential and a proton concentration gradient across the inner membrane. The movement of protons
569 back across the inner membrane, driven by this force, is coupled to the synthesis of ATP from ADP and
570 P_i by the ATP synthase. During SiO_2 nanoparticle perfusion (indicated by gray arrows), defects in the
571 mitochondrial homeostasis contribute to the energetic mismatch observed (ATP depletion). SiO_2
572 nanoparticles internalize and directly (dotted line) or indirectly produce ROS, such as the superoxide
573 radical ($O_2\cdot$), which is transformed to H_2O_2 by superoxide dismutase (SOD) and then converted to H_2O
574 using glutathione peroxidase activity (GPx), depleting the (GSH) and increasing oxidative stress. When a
575 cardiomyocyte is depolarized, Ca^{2+} enters through the L-type calcium channels (LTCC). This Ca^{2+} triggers
576 a subsequent release of Ca^{2+} that is stored in the sarcoplasmic reticulum (SR); through ryanodine
577 receptors (RyR2), the Ca^{2+} released by the SR increases the intracellular Ca^{2+} (lower Ca^{2+} SR release),
578 and then free Ca^{2+} binds to troponin C (TnC) and interacts with several proteins, which results in the
579 sarcomere length being shortened (cell shortening decrease). In the relaxation phase, the SR
580 sequesters Ca^{2+} using an ATP-dependent calcium pump (SERCA2a), which lowers the cytosolic Ca^{2+}
581 concentration and removes calcium from the TnC, but because of the energy depletion, SERCA reduces
582 its activity, which decreases the Ca^{2+} SR content.

583 **Clinical relevance**

584 The World Health Organization estimated that there would be about 20 million cardiovascular disease
585 deaths in 2015, accounting for 30% of all deaths worldwide. In this context, the likelihood of

cardiovascular diseases being associated with particulate air pollution is well documented. A series of scientific statements from the American Heart Association stressed that exposure to elevated levels of particulate matters is strongly linked with heart diseases, particularly when more than 75% of the total number of particles are nanoparticles (6, 17, 21). However, the correlation between heart disease and nanoscale particles is still being debated, and the related research conclusions lack consistency. Therefore, studying the cardiovascular toxicity of nanoscale particles is necessary and has profound scientific significance, particularly with regard to nanoparticle types, such as metal, metal-oxide, and carbon nanotubes, that have been reported to produce toxicity in other organs (35). To the best of our knowledge, we have demonstrated for the first time that SiO_2 nanoparticles impair the bioenergetics status and may consequently impact Ca^{2+} handling and contraction in rat cardiomyocytes. The mechanism of cardiotoxicity for SiO_2 particles mimics the pathological mechanisms of a failing heart. These findings will be helpful in managing risk and providing guidance to reduce the hazardous effects of nanoscale particles. In addition, a better understanding of the mechanism through which nanoparticles produce cardiotoxicity could uncover novel avenues for avoiding the side effects associated with the use of these particles.

In summary, the findings of this study support the notion that SiO_2-induced cardiomyocyte toxicity is strongly size dependent. 1) We showed differential, dose-dependent toxicity after 24 h incubation, with differential time-dependent cell death by necrosis (as shown by LDH leakage) and no activation of apoptosis. 2) We visualized, by confocal microscopy, an internalization phenomenon in these non-dividing, non-phagocytic primary-culture cell types, thus opening up a new field of study. 3) Our results showed the role of oxidative stress and the direct effect of SiO_2 particles on cell function: impaired Ca^{2+} handling and a reduction in cell shortening. These effects were all due to mitochondrial malfunction,

608 which is shown as a drop in the membrane potential and ATP content (Figure 11). These data enable us
609 to explore and carefully design new medical devices and clinical therapeutic protocols that take into
610 account the advantages and disadvantages of nanoparticles, in particular SiO_2.
611
612 **Acknowledgements**
613 We thank Dr. Tzarara López-Luke and María Christian Álbor Cortés (Centro de Investigaciones en
614 Óptica, CIO., Guanajuato. México), Lilia Magdalena Bautista Carrillo and Nayely Pineda Aguilar (Centro
615 de Investigación en Materiales Avanzados S.C.), and Dr. Flavio Contreras-Torres (Laboratorio de
616 Nanotecnología Ambiental, Tecnológico de Monterrey) for their technical support. We acknowledge
617 Valeria Oropeza for the design of figure 11.
618 **Source of Funding**
619 This work was partially supported by Endowed Chair in Cardiology (Tecnológico de Monterrey,
620 0020CAT131) as well as the CONACYT grant 151136, 133591, 269399 and Fronteras de la Ciencia grant
621 (0682) and Xignus Research Fund. Postdoctoral fellowship (CONACYT, 290885 to C.E.G.B). SEM-EDS
622 work was supported by grants from the National Center for Research Resources (5 G12RR013646-12)
623 and the National Institute on Minority Health and Health Disparities (G12MD007591) from the National
624 Institutes of Health.
625 **Disclosure**
626 The authors report no conflicts of interest. The authors alone are responsible for the content and
627 writing of the paper.
628
629

References

1. **Al-Rasheed NM, Faddah LM, Mohamed AM, Abdel Baky NA, Al-Rasheed NM, Mohammad RA.** Potential impact of quercetin and idebenone against immuno- inflammatory and oxidative renal damage induced in rats by titanium dioxide nanoparticles toxicity. *J Oleo Sci* 62:961-971, 2013.
2. **Arvizo RR, Miranda OR, Moyano DF, Walden CA, Giri K, Bhattacharya R, Robertson JD, Rotello VM, Reid JM, Mukherjee P.** Modulating pharmacokinetics, tumor uptake and biodistribution by engineered nanoparticles. *PLoS One* 6:e24374, 2011.
3. **Balderas-Villalobos J, Molina-Muñoz T, Mailloux-Salinas P, Bravo G, Carvajal K, Gómez-Viquez NL.** Oxidative stress in cardiomyocytes contributes to decreased SERCA2a activity in rats with metabolic syndrome. *Am J Physiol Heart Circ Physiol* 305: H1344-1353, 2013.
4. **Bers DM.** Cardiac excitation-contraction coupling. *Nature* 415:198-205, 2002. Review
5. **Blanco E, Hsiao A, Ruiz-Esparza GU, Landry MG, Meric-Bernstam F, Ferrari M.** Molecular-targeted nanotherapies in cancer: enabling treatment specificity. *Mol Oncol* 5:492-503, 2001.
6. **Brook RD, Rajagopalan S, Pope CA 3rd, Brook JR, Bhatnagar A, Diez-Roux AV, Holguin F, Hong Y, Luepker RV, Mittleman MA, Peters A, Siscovick D, Smith SC Jr, Whitsel L, Kaufman JD.** Particulate matter air pollution and cardiovascular disease. *Circulation* 121:2331-2378, 2010.
7. **Campbell JL.** GUPIX and GUPIXWIN. 2005. http://pixe.physics.uoguelph.ca/gupix/about/.
8. **Du Z, Zhao D, Jing L, Cui G, Jin M, Li Y, Liu X, Liu Y, Du H, Guo C, Zhou X, Sun Z.** Cardiovascular toxicity of different sizes amorphous silica nanoparticles in rats after intratracheal instillation. *Cardiovasc Toxicol* 13:194-207, 2013.

9. **Duan J, Yu Y, Li Y, Li Y, Liu H, Jing L, Yang M, Wang J, Li C, Sun Z.** Low-dose exposure of silica nanoparticles induces cardiac dysfunction via neutrophil-mediated inflammation and cardiac contraction in zebrafish embryos. *Nanotoxicology* 9:1-11, 2015.
10. **Duan J, Yu Y, Li Y, Yu Y, Sun Z.** Cardiovascular toxicity evaluation of silica nanoparticles in endothelial cells and zebrafish model. *Biomaterials* 34:5853-5862, 2013.
11. **Dzeja PP, Terzic A.** Phosphotransfer networks and cellular energetics. *J Exp Biol* 206:2039-2047, 2003.
12. **Endoh M.** Cardiac Ca2+ signaling and Ca2+ sensitizers. *Circ J* 72:1915-1925, 2008.
13. **Farcal LR, Uboldi C, Mehn D, Giudetti G, Nativo P, Ponti J, Gilliland D, Rossi F, Bal-Price A.** Mechanisms of toxicity induced by SiO2 nanoparticles of in vitro human alveolar barrier: effects on cytokine production, oxidative stress induction, surfactant proteins mRNA expression and nanoparticles uptake. *Nanotoxicology* 7:1095-1110, 2013.
14. **Fernández-Sada E, Silva-Platas C, Villegas CA, Rivero SL, Willis BC, García N, Garza JR, Oropeza-Almazán Y, Valverde CA, Mazzocchi G, Zazueta C, Torre-Amione G, García-Rivas G.** Cardiac responses to β-adrenoceptor stimulation is partly dependent on mitochondrial calcium uniporter activity. *Br J Pharmacol* 171:4207-4221, 2014.
15. **Gebel T, Marchan R, Hengstler JG.** The nanotoxicology revolution. *Arch Toxicol* 87:2057-2062, 2013.
16. **Gilardino A, Catalano F, Ruffinatti FA, Alberto G, Nilius B, Antoniotti S, Martra G, Lovisolo D.** Interaction of SiO2 nanoparticles with neuronal cells: Ionic mechanisms involved in the perturbation of calcium homeostasis. *Int J Biochem Cell Biol* 66:101-111, 2015.

17. **Gold DR, Mittleman MA.** New insights into pollution and the cardiovascular system: 2010 to 2012. *Circulation* 127:1903-1913, 2013.

18. **Gratton SE, Ropp PA, Pohlhaus PD, Luft JC, Madden VJ, Napier ME, DeSimone JM.** The effect of particle design on cellular internalization pathways. *Proc Natl Acad Sci U S A* 105:11613-8, 2014.

19. **Ide T, Tsutsui H, Kinugawa S, Utsumi H, Kang D, Hattori N, Uchida K, Arimura Ki, Egashira K, Takeshita A.** Mitochondrial electron transport complex I is a potential source of oxygen free radicals in the failing myocardium. *Circ Res* 85:357-363, 1999.

20. **Jakob AM, Schmedake TA.** A Novel Approach to Monodisperse, Luminescent Silica Spheres. *Chem Mater* 18:3173-3175, 2006.

21. **Kumar P, Robins A.** A review of the characteristics of nanoparticles in the urban atmosphere and the prospects for developing regulatory controls. *Atmos Environ* 44:5035-5052, 2010.

22. **Kuum M, Kaasik A, Joubert F, Ventura-Clapier R, Veksler V.** Energetic state is a strong regulator of sarcoplasmic reticulum Ca2+ loss in cardiac muscle: different efficiencies of different energy sources. *Cardiovasc Res* 83:89-96, 2009.

23. **Li Z, Barnes JC, Bosoy A, Stoddart JF, Zink JI.** Mesoporous silica nanoparticles in biomedical applications. *Chem Soc Rev* 41:2590-2605, 2012.

24. **Lin W, Huang YW, Zhou XD, Ma Y.** In vitro toxicity of silica nanoparticles in human lung cancer cells. *Toxicol Appl Pharmacol* 217:252-259, 2006.

25. **Lozano O, Mejia J, Masereel B, Toussaint O, Lison D, Lucas S.** Development of a PIXE analysis method for the determination of the biopersistence of SiC and TiC nanoparticles in rat lungs. *Nanotoxicology* 6:263-271, 2012.

26. **Lozano O, Mejia J, Piret JP, Saout C, Dogné JM, Toussaint O, Lucas S.** How does the deposited dose of oxide nanomaterials evolve in an in vitro assay? *Journal of Physics: Conference Series* 429:012013, 2013.

27. **Luo Z, Hu Y, Xin R, Zhang B, Li J, Ding X, Hou Y, Yang L, Cai K.** Surface functionalized mesoporous silica nanoparticles with natural proteins for reduced immunotoxicity. *J Biomed Mater Res A* 102:3781-3794, 2014.

28. **Maack C, Cortassa S, Aon MA, Ganesan AN, Liu T, O'Rourke B.** Elevated cytosolic Na+ decreases mitochondrial Ca2+ uptake during excitation-contraction coupling and impairs energetic adaptation in cardiac myocytes. *Circ Res* 99:172-182, 2006.

29. **MacDonnell SM, García-Rivas G, Scherman JA, Kubo H, Chen X, Valdivia H, Houser SR.** Adrenergic regulation of cardiac contractility does not involve phosphorylation of the cardiac ryanodine receptor at serine 2808. *Circ Res* 102:e65-72, 2008.

30. **Miller CR, Bondurant B, McLean SD, McGovern KA, O'Brien DF.** Liposome-cell interactions in vitro: effect of liposome surface charge on the binding and endocytosis of conventional and sterically stabilized liposomes. *Biochemistry* 37:12875-12883, 1998.

31. **Miragoli M, Novak P, Ruenraroengsak P, Shevchuk AI, Korchev YE, Lab MJ, Tetley TD, Gorelik J.** Functional interaction between charged nanoparticles and cardiac tissue: a new paradigm for cardiac arrhythmia?. *Nanomedicine (Lond)* 8:725-737, 2013.

32. **Monopoli MP, Walczyk D, Campbell A, Elia G, Lynch I, Bombelli FB, Dawson KA.** Physical−Chemical Aspects of Protein Corona: Relevance to in Vitro and in Vivo Biological Impacts of Nanoparticles. *J Am Chem Soc* 133:2525-2534, 2001.

33. **Napierska D, Thomassen LC, Lison D, Martens JA, Hoet PH.** The nanosilica hazard. *Part Fibre Toxicol* 7:39, 2010.

34. **Napierska D, Thomassen LC, Rabolli V, Lison D, Gonzalez L, Kirsch-Volders M, Martens JA, Hoet PH.** Size-dependent cytotoxicity of monodisperse silica nanoparticles in human endothelial cells. *Small* 5:846-853, 2009.

35. **Nel A, Xia T, Mädler L, Li N.** Toxic potential of materials at the nanolevel. *Science* 311:622-627, 2006.

36. **Olson RD, Gambliel HA, Vestal RE, Shadle SE, Charlier HA Jr, Cusack BJ.** Doxorubicin cardiac dysfunction: effects on calcium regulatory proteins, sarcoplasmic reticulum, and triiodothyronine. *Cardiovasc Toxicol* 5:269-283, 2005.

37. **Qhobosheane M, Santra S, Zhang P, Tan W.** Biochemically functionalized silica nanoparticles. *Analyst* 126:1274-1278, 2001.

38. **Rabolli V, Thomassen LC, Princen C, Napierska D, Gonzalez L, Kirsch-Volders M, Hoet PH, Huaux F, Kirschhock CE, Martens JA, Lison D.** Influence of size, surface area and microporosity on the in vitro cytotoxic activity of amorphous silica nanoparticles in different cell types. *Nanotoxicology* 4:307-318, 2010.

39. **Rahman I, Kode A, Biswas SK.** Assay for quantitative determination of glutathione and glutathione disulfide levels using enzymatic recycling method. *Nature Protocols* 1:3159-3165, 2006.

40. **Ruiz-Esparza GU, Cordero-Reyes AM, Youker KY, Serda RE, Yokoi K, Cara FE, Kirui DK, Paez-Mayorga J, Flores-Arredondo JH, Guerrero-Beltrán CE, García-Rivas G, Ferrari M, Blanco E,**

Torre-Amione G. A specifically designed nanoconstruct associates, internalizes, traffics in cardiovascular cells and accumulates in failing myocardium. *Eur J Heart Fail* 18:169-178, 2016.

41. **Savi M, Rossi S, Bocchi L, Gennaccaro L, Cacciani F, Perotti A, Amidani D, Alinovi R, Goldoni M, Aliatis I, Lottici PP, Bersani D, Campanini M, Pinelli S, Petyx M, Frati C, Gervasi A, Urbanek K, Quaini F, Buschini A, Stilli D, Rivetti C, Macchi E, Mutti A, Miragoli M, Zaniboni M.** Titanium dioxide nanoparticles promote arrhythmias via a direct interaction with rat cardiac tissue. *Early Hum Dev* 11:63, 2014.
42. **Serda RE, Godin B, Blanco E, Chiappini C, Ferrari M.** Multi-stage delivery nano-particle systems for therapeutic applications. *Biochim Biophys Acta* 1810:317-329, 2011.
43. **Serda RE, Gu J, Bhavane RC, Liu X, Chiappini C, Decuzzi P, Ferrari M.** The association of silicon microparticles with endothelial cells in drug delivery to the vasculature. *Biomaterials* 30:2440-2448, 2009.
44. **Silva-Platas C, Guerrero-Beltrán CE, Carrancá M, Castillo EC, Bernal-Ramírez J, Oropeza-Almazán Y, González LN, Rojo R, Martínez LE, Valiente-Banuet J, Ruiz-Azuara L, Bravo-Gómez ME, García N, Carvajal K, García-Rivas G.** Antineoplastic copper coordinated complexes uncouple oxidative phosphorylation and induce mitochondrial permeability transition in cardiac mitochondria and cardiomyocytes. *J Bioenerg Biomembr* 48:43-54, 2016.
45. **Sohaebuddin SK, Thevenot PT, Baker D, Eaton JW, Tang L.** Nanomaterial cytotoxicity is composition, size, and cell type dependent. *Part Fibre Toxicol* 7:22, 2010.
46. **Sotiriou GA, Diaz E, Long MS, Godleski J, Brain J, Pratsinis SE, Demokritou P.** A novel platform for pulmonary and cardiovascular toxicological characterization of inhaled engineered nanomaterials. *Nanotoxicology* 6:680-690, 2012.

757 47. **Sun L, Li Y, Liu X, Jin M, Zhang L, Du Z, Guo C, Huang P, Sun Z.** Cytotoxicity and mitochondrial
758 damage caused by silica nanoparticles. *Toxicol In Vitro* 25:1619-1629, 2011.
759 48. **Szebeni J, Alving CR, Rosivall L, Bünger R, Baranyi L, Bedöcs P, Tóth M, Barenholz Y.** Animal
760 models of complement-mediated hypersensitivity reactions to liposomes and other lipid-based
761 nanoparticles. *J Liposome Res* 17:107-117, 2007.
762 49. **Tang L, Cheng J.** Nonporous silica nanoparticles for nanomedicine application. *Nano Today*
763 8:290-312, 2013.
764 50. **Tasciotti E, Liu X, Bhavane R, Plant K, Leonard AD, Price BK, Cheng MM, Decuzzi P, Tour JM,**
765 **Robertson F, Ferrari M.** Mesoporous silicon particles as a multistage delivery system for
766 imaging and therapeutic applications. *Nat Nanotechnol* 3:151-157, 2008.
767 51. **Wang Y, Zhao Q, Han N, Bai L, Li J, Liu J, Che E, Hu L, Zhang Q, Jiang T, Wang S.** Mesoporous
768 silica nanoparticles in drug delivery and biomedical applications. *Nanomedicine*11:313-327,
769 2015.
770 52. **Williams GS, Boyman L, Lederer WJ.** Mitochondrial calcium and the regulation of metabolism in
771 the heart. *J Mol Cell Cardiol* 8:35-45, 2015.
772 53. **Willis BC, Salazar-Cantú A, Silva-Platas C, Fernández-Sada E, Villegas CA, Rios-Argaiz E,**
773 **González-Serrano P, Sánchez LA, Guerrero-Beltrán CE, García N, Torre-Amione G, García-Rivas**
774 **GJ, Altamirano J.** Impaired oxidative metabolism and calcium mishandling underlie cardiac
775 dysfunction in a rat model of post-acute isoproterenol-induced cardiomyopathy. *Am J Physiol*
776 *Heart Circ Physiol* 308:H467-477, 2015.

54. **Xue Y, Chen Q, Ding T, Sun J.** SiO_2 nanoparticle-induced impairment of mitochondrial energy metabolism in hepatocytes directly and through a Kupffer cell-mediated pathway in vitro. *Int J Nanomedicine* 9:2891-2903, 2014.

55. **Zarain-Herzberg A, García-Rivas G, Estrada-Avilés R.** Regulation of SERCA pumps expression in diabetes. *Cell Calcium* 56:302-310, 2014.

Figure Captions

Figure 1. Characterization of silica particles by SEM, XRD, DLS and zeta potential. A) Representative Micro-SiO_2 micrograph showing size and morphology. Insert shows size distribution of Micro-SiO_2 obtained by FEG-SEM (n=100 particles). B) X-ray diffraction (XRD) analysis with the composition of the talline domains of Nano- and Micro-SiO_2. All samples show the characteristic diffraction pattern of amorphous silica presenting a broad peak (10-30º) with a maximum around 22 º. C) The hydrodynamic sizes of Nano- and Micro-SiO_2 particles in ultrapure water D) The zeta potentials of Nano- and Micro-SiO_2 particles in ultrapure water. Colors black and gray corresponding to Micro-SiO_2 and Nano-SiO_2 respectively in each graphic.

Figure 2. Viability of adult cardiomyocytes after 24 h exposure of SiO_2 particles and mechanism of cell death.

A) Nano-SiO_2 and Micro-SiO_2 viability evaluated by Alamar Blue viability test. B) Representative dot-plots from flow cytometry with AnnexinV-PE-Cy7/Ghost Red 780 cell death analysis. A positive control of apoptosis cell death (56°C for 10 mins) is shown in comparison to CT, Nano-SiO_2 and Micro-SiO_2

798 treated groups at 99.5 μg/ml. C) The percentage of necrotic, live and apoptotic cells was quantified and
799 is shown in the bar graph. D) Time-dependent cytotoxicity by Lactate dehydrogenase (LDH) leakage at
800 0-24 hours, in cultured cardiomyocytes with 24 hours incubation of Nano-SiO_2 and Micro-SiO_2 at its IC_{50}
801 (99.5 μg/ml for Nano and 1,500 μg/ml for Micro-SiO_2 particles). Values are mean ± SEM, n=3-10;
802 *p<0.05; **p<0.01; ***p<0.001 vs. control (CT).
803
804 **Figure 3. SiO_2 cellular association and internalization in adult rat cardiomyocytes.** Representative
805 SEM micrographs showing: A) Nano-SiO_2 and B) Micro-SiO_2 individual and agglomerates/aggregates
806 association to the cellular membrane. Representative SEM-EDS transversal cut images of C) untreated
807 D) Nano-SiO_2 and E) Micro-SiO_2 particle internalization after 24h of incubation (99.5 μg/ml). F)
808 Quantification of internalized SiO_2 particles by PIXE, as a function of time (for Nano 99.5 μg/ml and
809 Micro-SiO_2 1,500 μg/ml). G) Representative confocal microscopy image of the F-Micro-SiO_2 shown as x,
810 y and z-stacks. The cytoskeleton is shown in red and the brighter dots correspond to F-Micro-SiO_2
811 particles. The arrows indicate the SiO_2 particles in the cell. The symbol N (in panel G) marks the nucleus
812 location in the cell. Values are mean ± SD, a t-test was used as statistical analysis between Nano- and
813 Micro-SiO_2. Values are mean ± SEM, n=3-5. *p<0.05 vs. Nano; ‡p<0.05 vs. basal (time 0).
814
815 **Figure 4. Cardiomyocytes surface showing Silica particles by energy-dispersive X-ray spectroscopy**
816 **(EDS).** Right, FEG-SEM images of A) Micro-SiO_2 and B) Nano-SiO_2 individual and
817 agglomerates/aggregates association to the cellular membrane and C) an adult rat cardiomyocyte as a
818 control sample. Left, the respective four EDS-images of elemental maps for carbon (red), sodium
819 (cyan), silicon (magenta/yellow) and oxygen (green).

Figure 5. Micro-SiO_2 internalization in adult myocytes. A) Semi-quantitative increase in fluorescence in a dose-dependent manner of F-Micro-SiO_2 particles. B) Representative images from ventricular myocytes at the control (CT) condition and 150 μg/ml F-Micro-SiO_2 concentration. The cytoskeleton is shown in red and F-Micro-SiO_2 in green. Values are mean ± SEM, n=4-6. *p<0.05 *vs*. CT.

Figure 6. Cell shortening and Ca^{2+} handling in cardiomyocytes treated with Nano- and Micro-SiO_2 particles. The percentage of cell shortening before (CT) and after a 24 h treatment of Nano-SiO_2 and Micro-SiO_2 at its $IC_{50.}$ Values are mean ± SEM, n=15. **p<0.001 *vs.* CT.

Figure 7. Calcium transient characterization at basal condition and after β-adrenergic stimulation. A-B) Representative images from field stimulated control and Nano-SiO_2 treated myocytes under basal conditions and after isoproterenol (ISO) perfusion, the arrow indicates the analyzed transient for semi-quantitative results. C) Peak Ca^{2+} transient amplitude. D) Time to 50% of decay ($T_{50\%}$). Values are mean ± SEM. CT: n=22-33 cells/3 animals; Nano-SiO_2: n=19-34 cells/3 animals *p<0.05 *vs*. Nano-SiO_2; ‡‡p<0.001 *vs.* Basal.

Figure 8. Calcium sparks characterization in isolated myocytes. A) Line scan images from control conditions (left) and after 24 hours incubation with Nano-SiO_2 (right). Surface plots can be seen above line scan images. Line profiles from selected 2 μm regions (black marks in line scan images) can be seen

on images. Pooled data describing B) spark frequency and C) amplitude. Values are mean ± SEM, n=39 cells/3 animals/CT; 33 cells/3 animals/Nano-SiO_2). *p<0.05 *vs.* CT.

Figure 9. Calcium content in the sarcoplasmic reticulum. Representative images from caffeine-induced Ca^{2+} transients from A) control (CT) and B) Nano-SiO_2 treated cardiomyocytes. Black arrow indicates caffeine application (10 mM). C) Pooled data for peak Ca^{2+} transient amplitude (sarcoplasmic reticulum, SR Load; n=25 cells/3 animals/CT; 24 cells/3 animals/Nano-SiO_2).

Figure 10. Mitochondrial membrane potential, ATP content, ROS production, and GSH depletion. Representative images from A) control (CT) and B) Nano-SiO_2 treated cardiomyocytes loaded with TMRE by confocal microscopy. Relative fluorescence from C) mitochondrial membrane potential (%) and D) ATP content (luminescence relative units, LRU) from control (CT) and Nano-SiO_2 treated cardiomyocytes. E) H_2O_2 production and F) Glutathione content, in cultured cardiomyocytes with 24 hours incubation of Nano-SiO_2 at its IC_{50}. Values are mean ± SEM, n=10-11 cells (A-D); n=3 (E and F); *p<0.05 *vs*. control (CT).

Figure 11. Proposed mechanism of SiO_2- induced cardiotoxicity. Scheme of the suggested mechanism by which Nano-SiO_2 particles induces cardiotoxicity interfering with energetic status and Ca^{2+} handling in cardiomyocytes. GSH/GSSG, reduced/oxidized glutathione; NCLX, Na+/Ca2+ exchanger; O2·, superoxide radical; LTCC, L-type calcium channels; SR, sarcoplasmic reticulum; RyR2, ryanodine receptors; TnC, troponin C.

862 **Table**

863 **Table 1. Characterization of silica particles by different techniques.**

Particle SiO_2	**Crystallinity** (XRD)	**Purity** (EDS) (%)	**Size distribution**		**Surface charge** (Zeta Potential) (mV)
			Feret diameter (FEG-SEM) (nm)	**Hydrodynamic diameter** (DLS) (nm)	
Nano-SiO_2	Amorphous	> 95%	7 *	91 ± 22 (water) 120 ± 25 (Tyrode) 220 ± 50 (M-199) 220 ± 106 (M-199 + BSA)	-24.1 (water) -22.0 (Tyrode) -21.6 (M-199) -20.8 (M-199 + BSA)
Micro-SiO_2	Amorphous	> 95%	666 ± 32	712 ± 212 (water) 1106 ± 281 (Tyrode) 1190 ± 272 (M-199) 1281 ± 488 (M-199 + BSA)	-14.4 (water) -19.5 (Tyrode) -18.8 (M-199) -12.3 (M-199 + BSA)
F- Micro-SiO_2	Amorphous	> 95%	611 ± 22	712 ± 153 (water) 712 ± 152 (Tyrode) 1484 ± 294 (M-199) 1484 ± 812 (M-199 + BSA)	-33.6 (water) -17.5 (Tyrode) -13.4 (M-199) -12.9 (M-199 + BSA)

864

865 XRD, X-ray Diffraction; EDS, Energy-dispersive X-ray spectroscopy; FEG-SEM, field emission gun

866 scanning electron microscope; DLS, Dynamic Light Scattering; ELS, Electrophoretic Light Scattering.

867 BSA: 5 mg/mL * Size as referred by the provider´s data sheet.

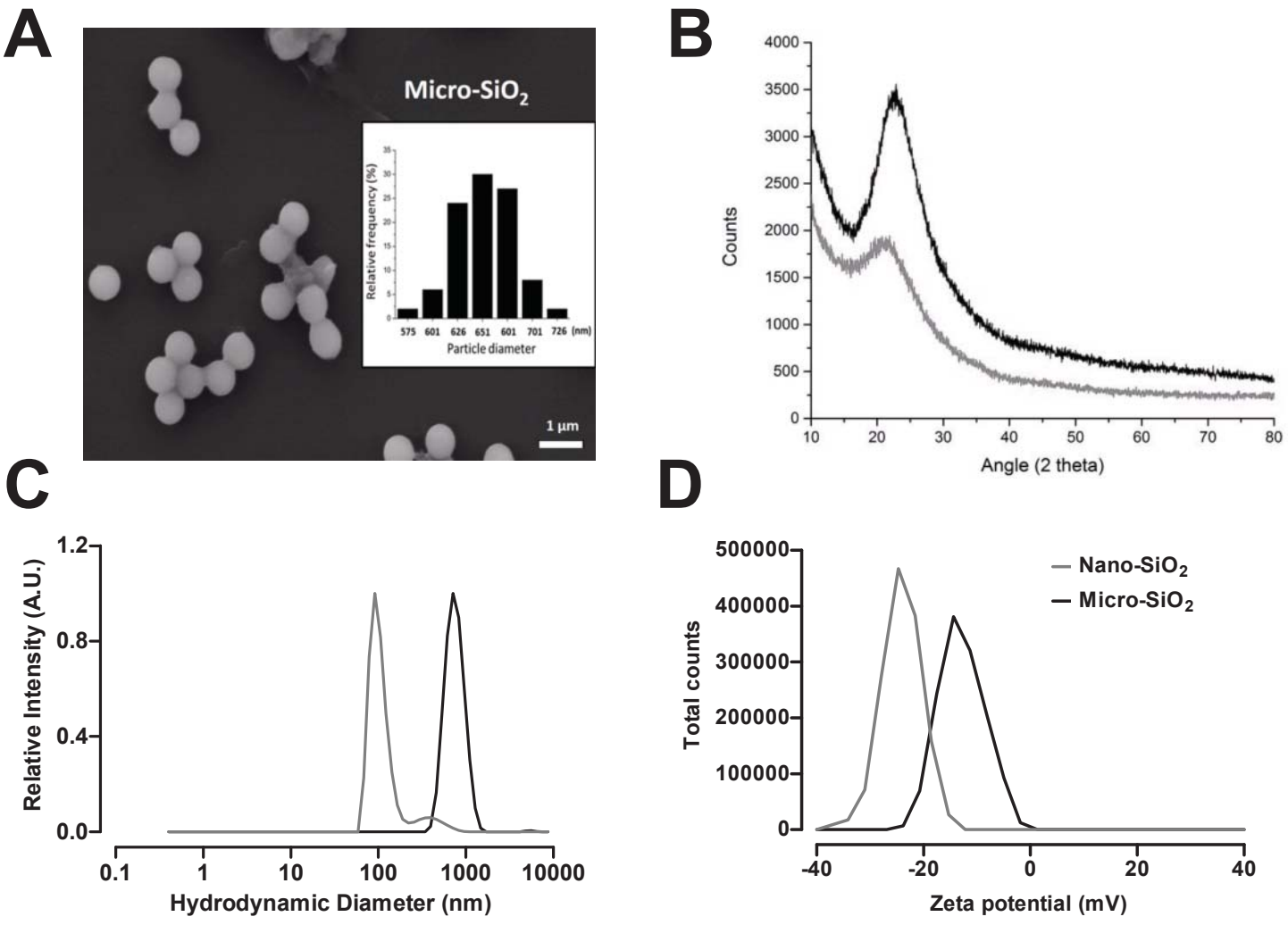
A
Micro-SiO2
Relative frequency (%)
575 601 626 651 601 701 726 (nm)
Particle diameter
1 µm
B
Counts
Angle (2 theta)
C
Relative Intensity (A.U.)
Hydrodynamic Diameter (nm)
D
Total counts
Zeta potential (mV)
Nano-SiO2
Micro-SiO2

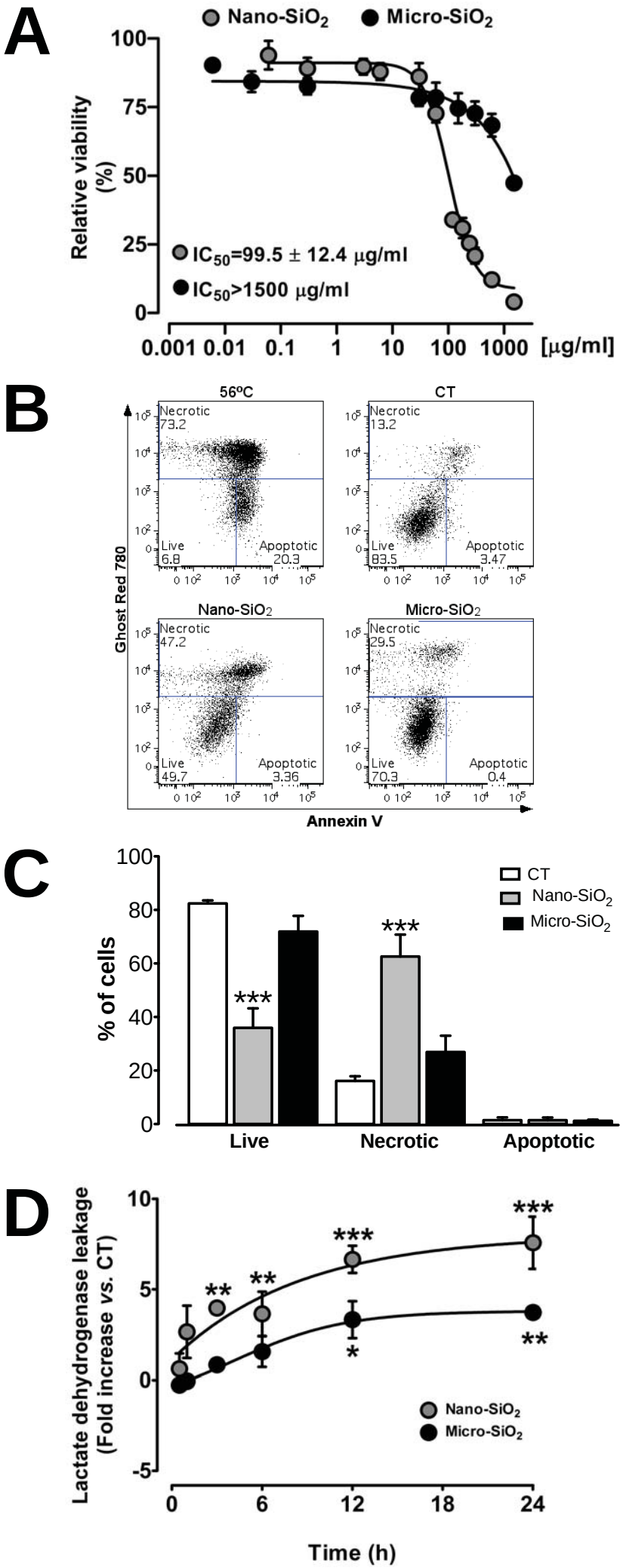
A
Nano-SiO2
Micro-SiO2
Relative viability (%)
100
75
50
25
0
IC50=99.5 ± 12.4 µg/ml
IC50>1500 µg/ml
0.001 0.01 0.1 1 10 100 1000 [µg/ml]
B
56ºC
CT
Nano-SiO2
Micro-SiO2
Necrotic
73.2
Live
6.8
Apoptotic
20.3
Necrotic
13.2
Live
83.5
Apoptotic
3.47
Necrotic
47.2
Live
49.7
Apoptotic
3.36
Necrotic
29.5
Live
70.3
Apoptotic
0.4
Ghost Red 780
Annexin V
C
CT
Nano-SiO2
Micro-SiO2
% of cells
100
80
60
40
20
0
***
***
Live
Necrotic
Apoptotic
D
Lactate dehydrogenase leakage (Fold increase vs. CT)
10
5
0
-5
**
**
***
*
***
**
Nano-SiO2
Micro-SiO2
0
6
12
18
24
Time (h)

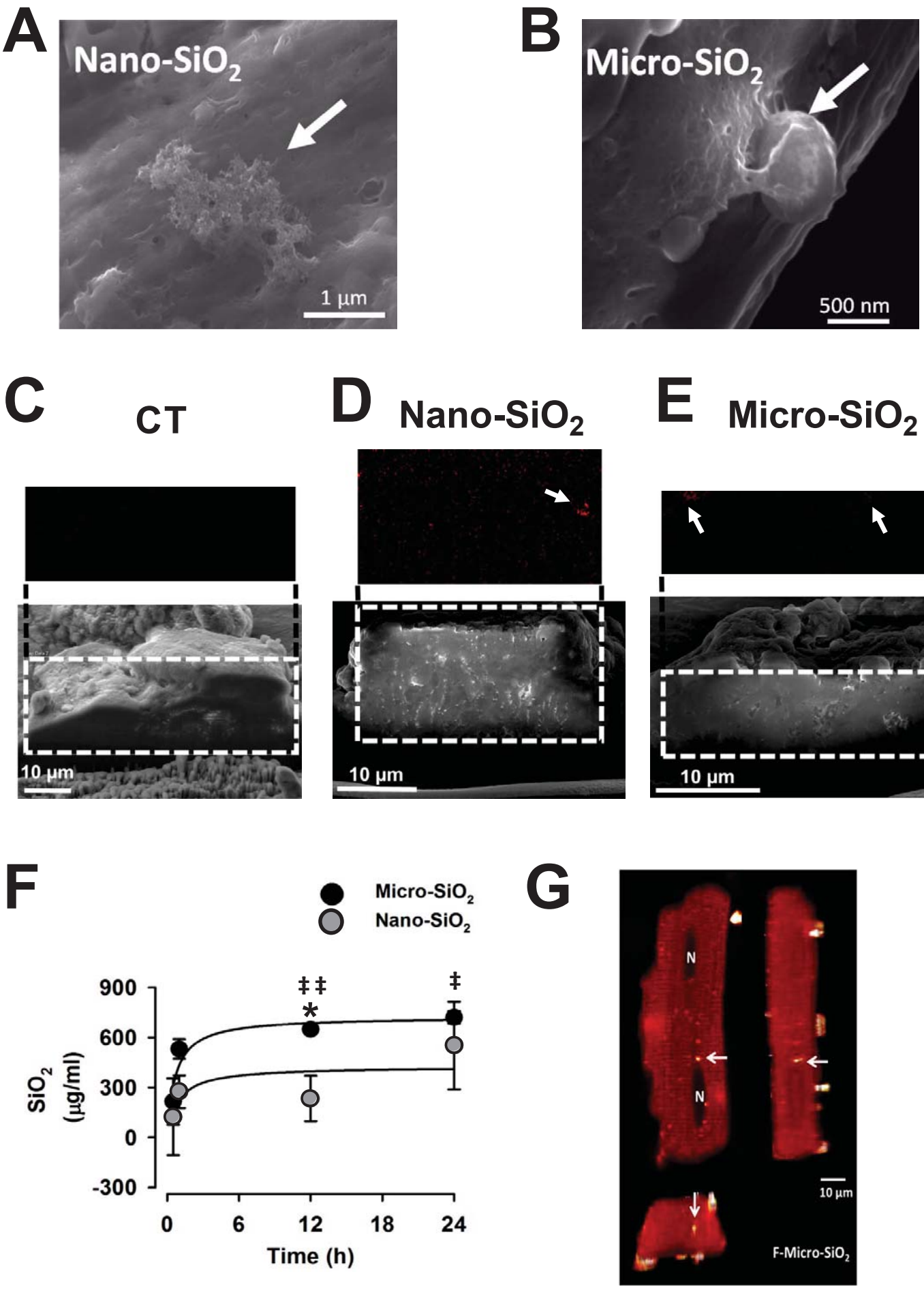
A
Nano-SiO2
1 μm
B
Micro-SiO2
500 nm
C
CT
D
Nano-SiO2
E
Micro-SiO2
10 μm
10 μm
10 μm
F
Micro-SiO2
Nano-SiO2
900
600
300
0
-300
SiO2 (μg/ml)
0
6
12
18
24
Time (h)
‡‡
*
‡
G
N
N
10 μm
F-Micro-SiO2

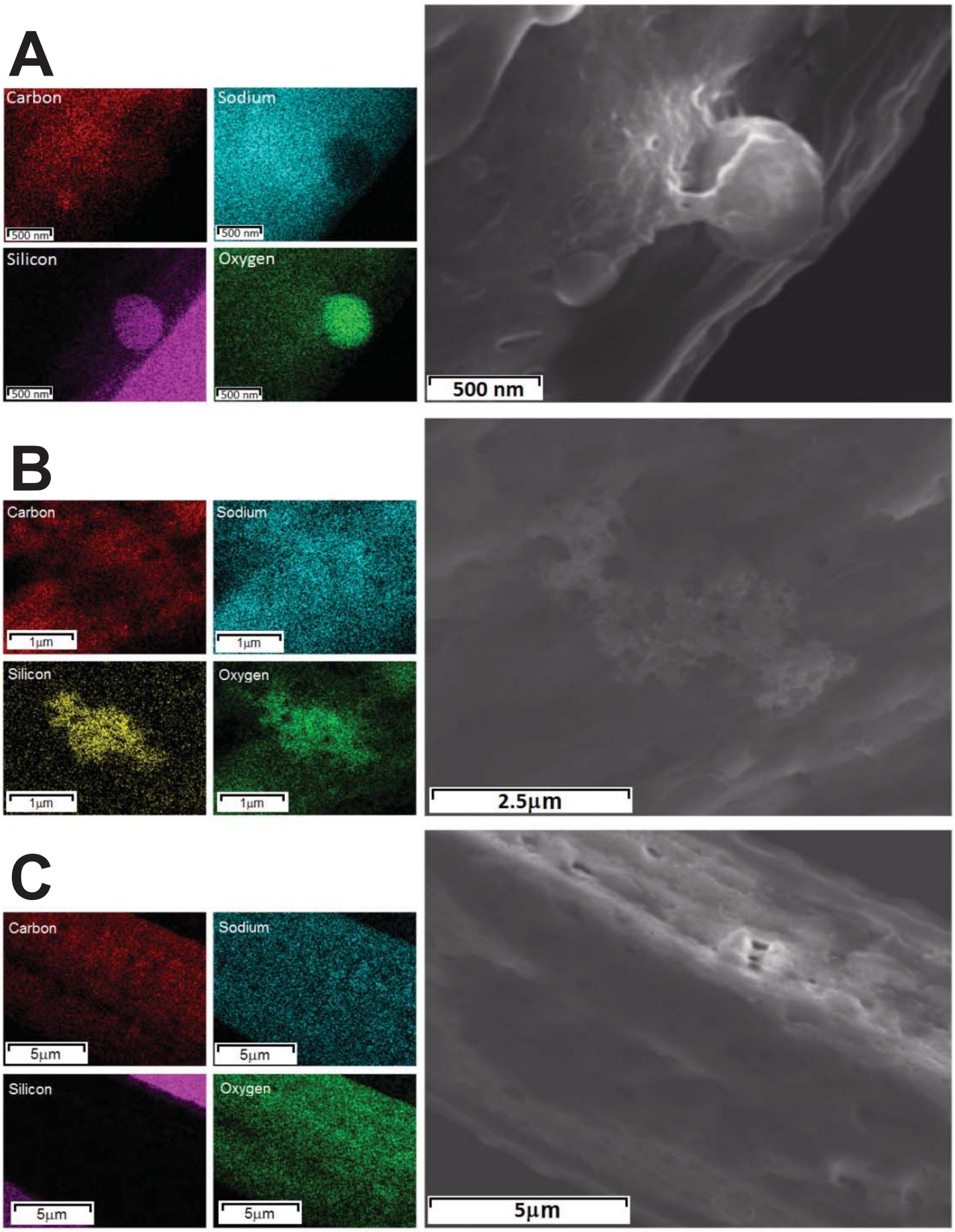
A
Carbon
Sodium
Silicon
Oxygen
500 nm
500 nm
500 nm
500 nm
500 nm
B
Carbon
Sodium
Silicon
Oxygen
1µm
1µm
1µm
1µm
2.5µm
C
Carbon
Sodium
Silicon
Oxygen
5µm
5µm
5µm
5µm
5µm

A

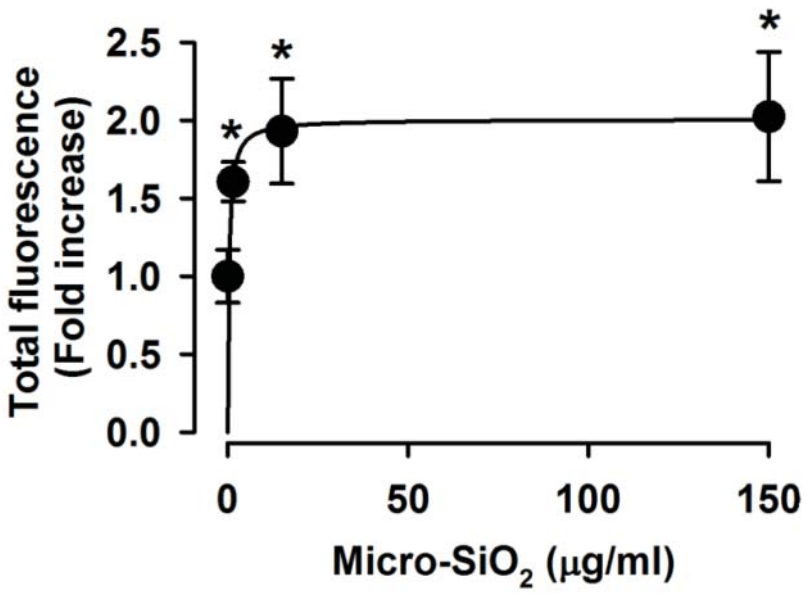
Total fluorescence
(Fold increase)
2.5
2.0
1.5
1.0
0.5
0.0
*
*
*
0
50
100
150
Micro-SiO2 (μg/ml)

B

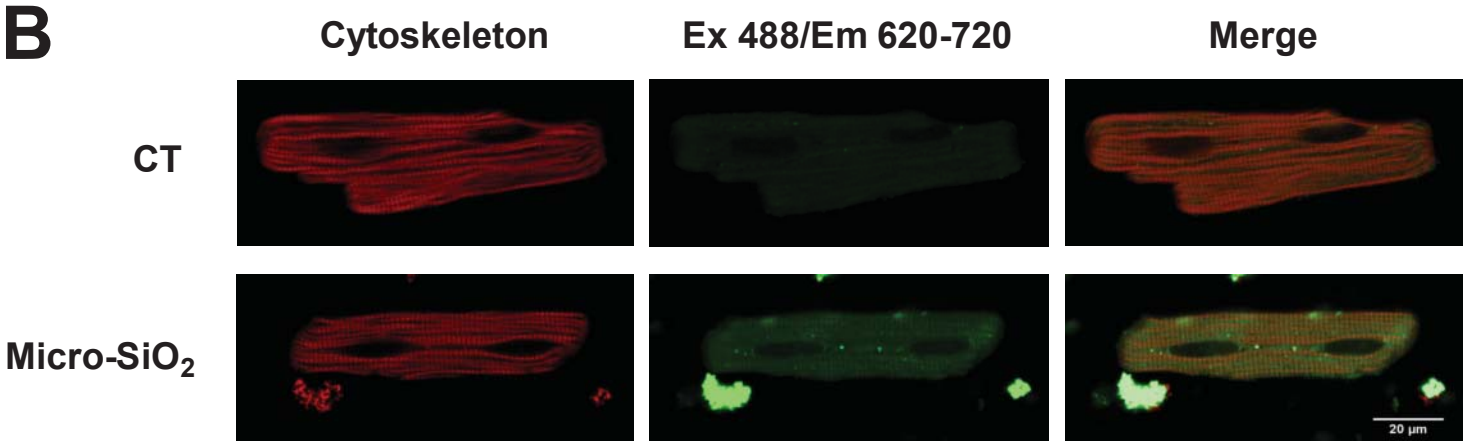
Cytoskeleton
Ex 488/Em 620-720
Merge
CT
Micro-SiO2
20 μm

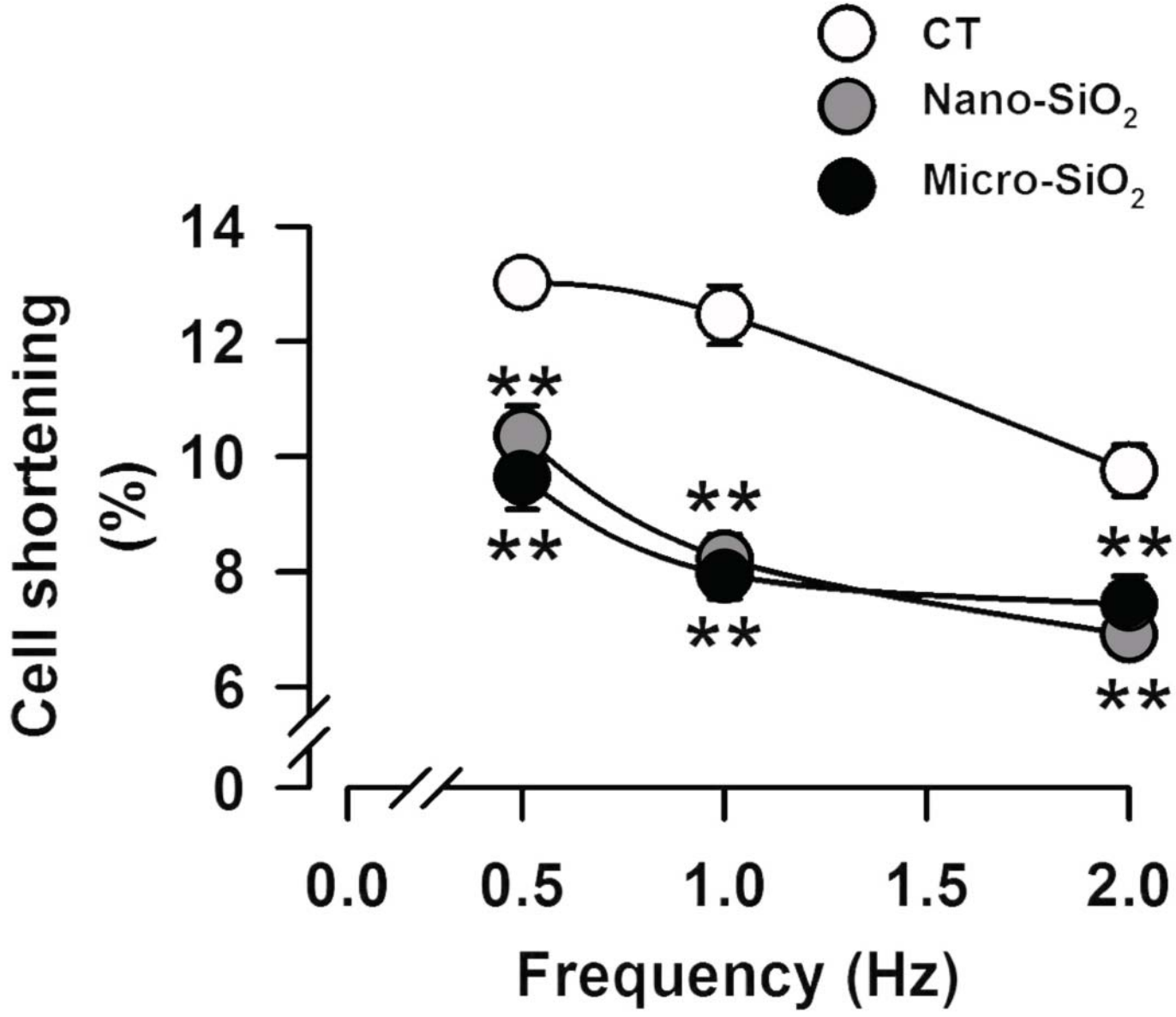
CT
Nano-SiO2
Micro-SiO2
Cell shortening
(%)
14
12
10
8
6
0
**
**
**
**
**
0.0
0.5
1.0
1.5
2.0
Frequency (Hz)

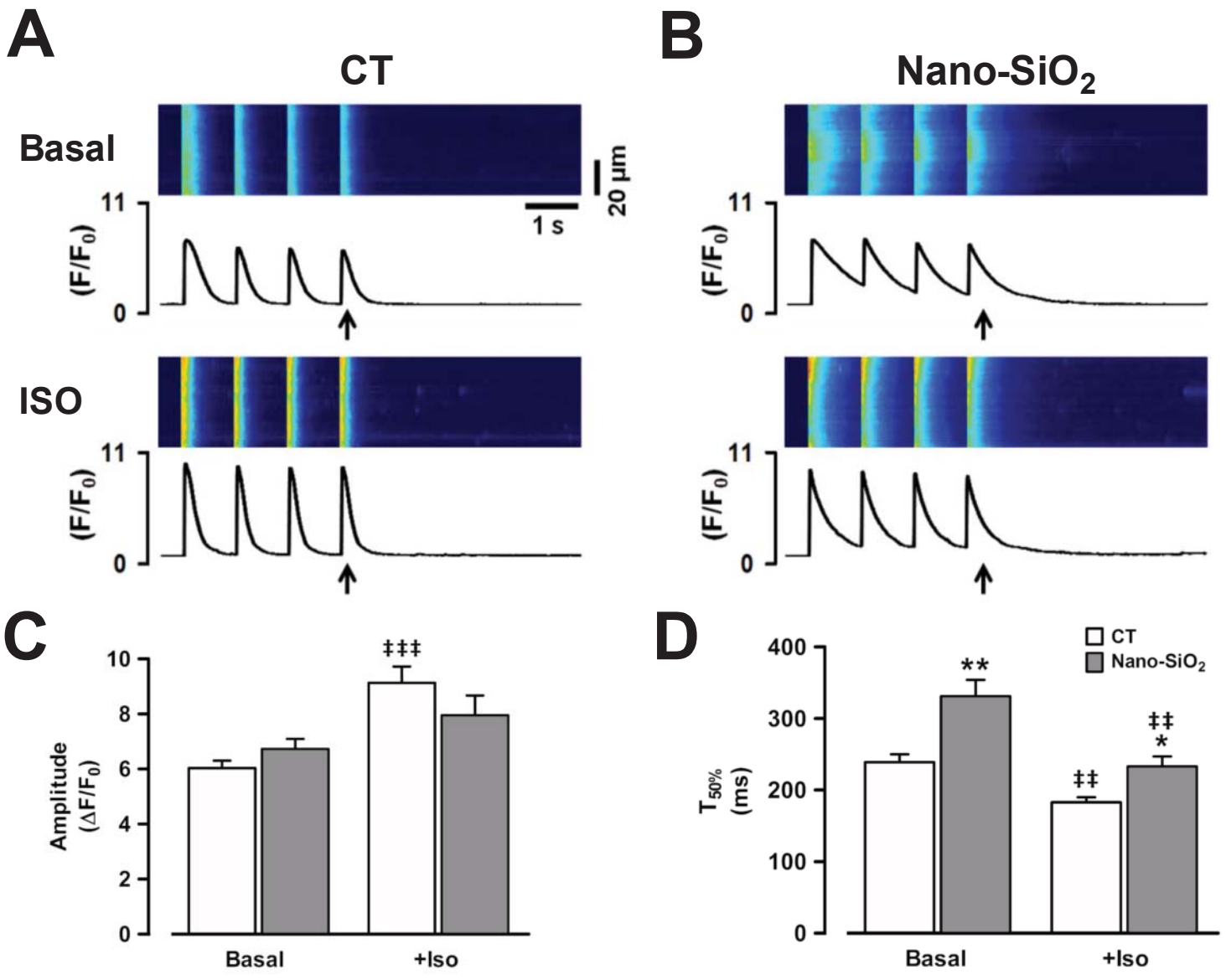
A
CT
Basal
20 µm
1 s
11
(F/F0)
0
ISO
B
Nano-SiO2
C
Amplitude (ΔF/F0)
10
8
6
4
2
0
‡‡‡
Basal
+Iso
D
CT
Nano-SiO2
T50% (ms)
400
300
200
100
0
**
‡‡
*
Basal
+Iso

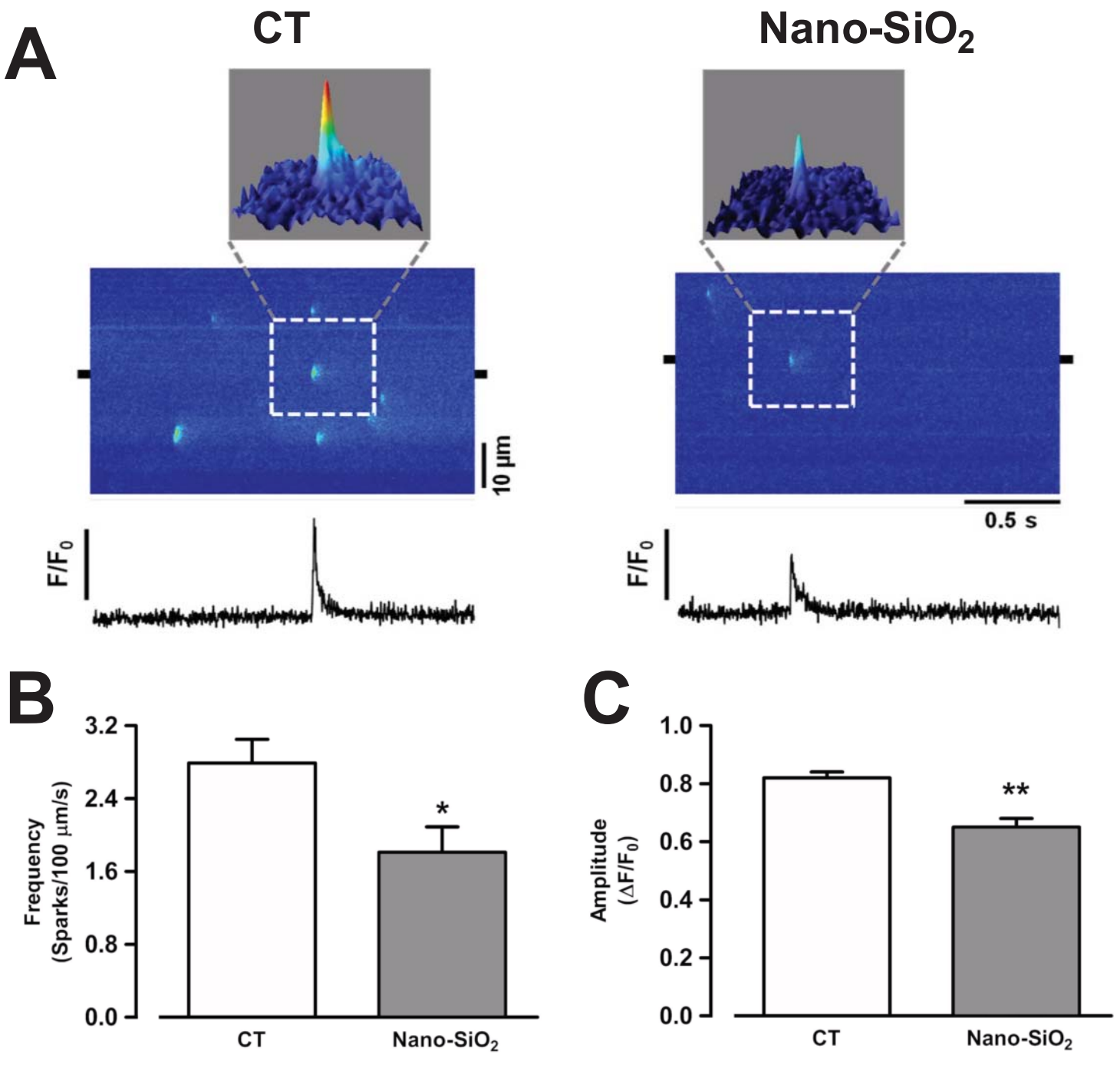
A
CT
Nano-SiO2
10 μm
0.5 s
F/F0
F/F0
B
Frequency (Sparks/100 μm/s)
3.2
2.4
1.6
0.8
0.0
*
CT
Nano-SiO2
C
Amplitude (ΔF/F0)
1.0
0.8
0.6
0.4
0.2
0.0
**
CT
Nano-SiO2

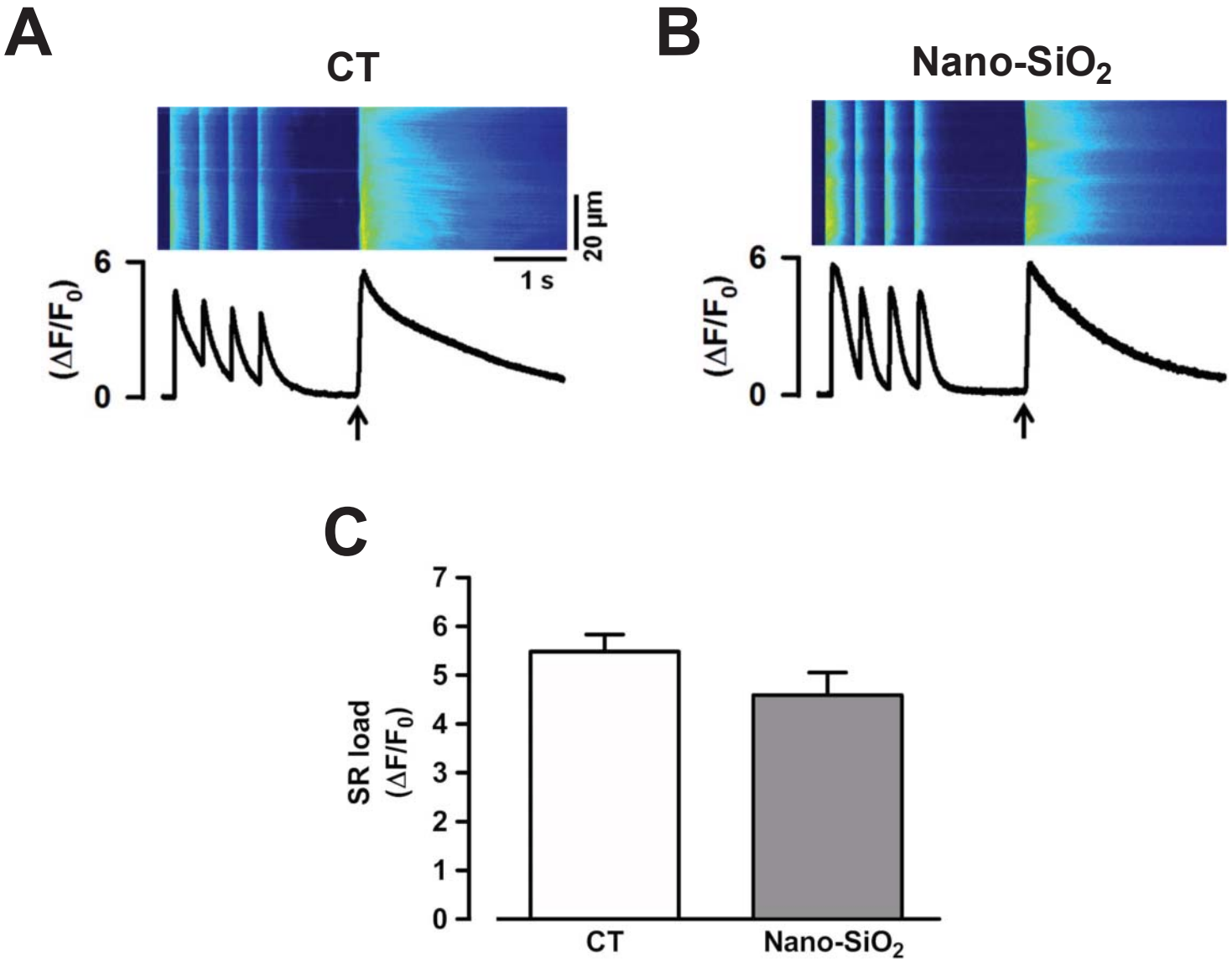
A
CT
20 μm
1 s
6
0
(ΔF/F0)
B
Nano-SiO2
6
0
(ΔF/F0)
C
SR load
(ΔF/F0)
7
6
5
4
3
2
1
0
CT
Nano-SiO2

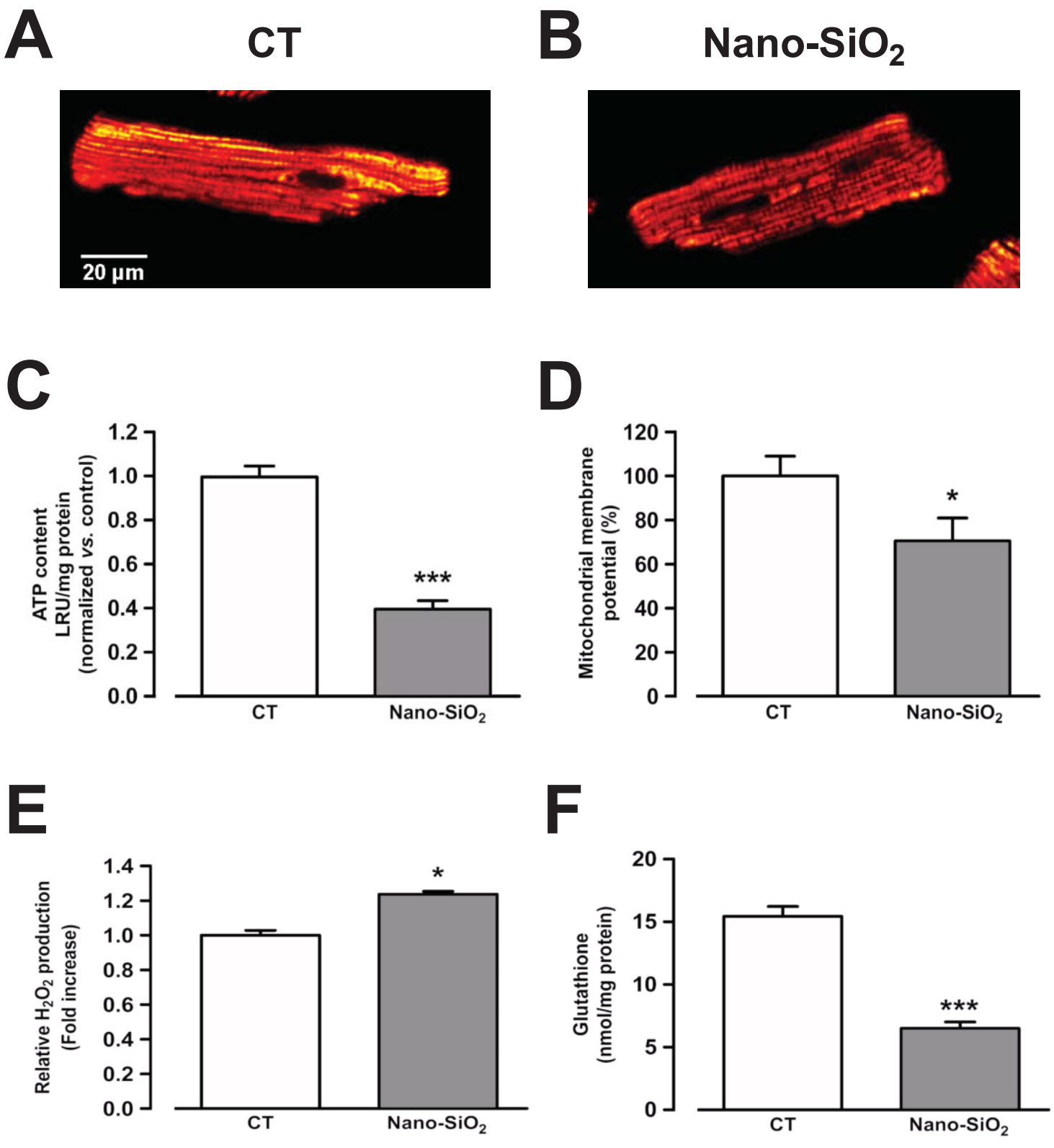
A
CT
B
Nano-SiO2
20 μm
C
ATP content
LRU/mg protein
(normalized vs. control)
1.2
1.0
0.8
0.6
0.4
0.2
0.0
***
CT
Nano-SiO2
D
Mitochondrial membrane
potential (%)
120
100
80
60
40
20
0
*
CT
Nano-SiO2
E
Relative H2O2 production
(Fold increase)
1.4
1.2
1.0
0.8
0.6
0.4
0.2
0.0
*
CT
Nano-SiO2
F
Glutathione
(nmol/mg protein)
20
15
10
5
0
***
CT
Nano-SiO2